

# Dynamic Response of Novel Adaptive Modified Recurrent Legendre Neural Network Control for PMSM Servo-Drive Electric Scooter

DOI 10.7305/automatika.2015.07.753  
UDK 629.32-025.26:004.273

Original scientific paper

Because an electric scooter driven by permanent magnet synchronous motor (PMSM) servo-driven system has the unknown nonlinearity and the time-varying characteristics, its accurate dynamic model is difficult to establish for the design of the linear controller in whole system. In order to conquer this difficulty and raise robustness, a novel adaptive modified recurrent Legendre neural network (NN) control system, which has fast convergence and provide high accuracy, is proposed to control for PMSM servo-driven electric scooter under the external disturbances and parameter variations in this study. The novel adaptive modified recurrent Legendre NN control system consists of a modified recurrent Legendre NN control with adaptation law and a remunerated control with estimation law. In addition, the online parameter tuning methodology of the modified recurrent Legendre NN control and the estimation law of the remunerated control can be derived by using the Lyapunov stability theorem and the gradient descent method. Furthermore, the modified recurrent Legendre NN with variable learning rate is proposed to raise convergence speed. Finally, comparative studies are demonstrated by experimental results in order to show the effectiveness of the proposed control scheme.

**Key words:** Permanent magnet synchronous motor, Legendre neural network, Lyapunov stability

**Dinamički odziv nove adaptivne modificirane povratne Legendrove neuronske mreže upravljanja sinkronim motorom s permanentnim magnetima za električni skuter.** S obzirom da električni skuter pogonjen servo sustavom sa sinkroni motor s permanentnim magnetima ima nelinearnu dinamiku i vremenski promjenjive parametre, njegov dinamički model nije jednostavno odrediti u svrhu dizajniranja linearnog regulatora. Kako bi se riješio taj problem te povećala robusnost predložen je sustav upravljanja korištenjem adaptivne modificirane povratne Legendrove neuronske mreže za upravljanje skuterom pogonjenim servo sustavom sa sinkronim motorom uz prisustvo vanjskog poremećaja i promjenjivih parametara. Predloženo upravljanje ima brzu konvergenciju i visoku preciznost. Sustav upravljanja sastoji se od modificirane povratne Legendrove neuronske mreže s adaptivnim zakonom upravljanja i estimacijom. Dodatno, *on-line* podešavanje parametara takvog sustava može se dobiti korištenjem Ljapunovljevog teorema o stabilnosti sustava i gradijente metode. Modificirana povratne Legendrove neuronska mreža s promjenjivim vremenom učenja predložena je za povećanje brzine konvergencije. Ispravnost predložene sheme upravljanja provjerena je eksperimentalno.

**Ključne riječi:** sinkroni motor s permanentnim magnetima, Legendrova neuronska mreža, stabilnost po Ljapunovu

## 1 INTRODUCTION

For the purpose of reducing air pollution and enhancing environmental protection, a few countries require their automotive industries to develop electric vehicles in place of gasoline-powered automobiles one by one. Because scooters are much more extensive than cars for personal transportation in Taiwan, I have been studying the development and research of the electric scooter. Since the wheels of the electric scooters are driven by AC motor, the selection of the AC motor drive system is a very important job. Owing to demand of high power density and high efficiency, the

selections of AC motor drive system are very important for the purpose of electric scooter driven by AC motor. Comparing permanent magnet synchronous motors (PMSMs) with other AC motors, PMSMs have many advantages, such as high power density, high efficiency, high robustness, etc. Therefore they have been widely used in many applications of mechatronics [1-3].

Artificial neural networks (NNs) have emerged as a powerful learning technique to perform complex tasks in highly nonlinear dynamic systems and controls [4-8]. Some of the prime advantages of using NN are: their abil-

ity to learn based on optimization of an appropriate error function and their excellent performance for approximation of nonlinear functions. There are different paradigms of NNs proposed by different researchers for the task of system identification and control [5-8]. One of the major drawbacks of the NN is that it is computationally intensive and needs large number of iterations for its training. In order to reduce the computational complexity, a functional-link NN, which shown that it is capable of producing similar performance as that of NN but with much less computational cost, is shown in [9-10]. Moreover, the functional-link NN-based nonlinear dynamic system identification with satisfactory results has been reported in [11]. It is shown that the performance of functional-link NN is similar to that of a NN but with faster convergence and lesser computational complexity. Moreover, a comprehensive survey on various applications of functional-link NN has been proposed in [12].

A novel Legendre polynomial based linear NN for static function approximation is proposed by Yang et al. [13]. They have shown that this network has fast convergence, and provide high accuracy. Recently, a Legendre polynomial NN for channel equalization problem has been proposed in [14-15]. It is shown that the superior performance of Legendre NN equalizer over the NN-based and RBF-based equalizers for different nonlinear channel models. Moreover, the computational complexity of Legendre NN is lower than the functional-link NN since the evaluation of Legendre polynomials involves less computation than the evaluation of trigonometric functions [16]. In addition, the predictive approach is based on Legendre neural network and a random time strength function via a promising data mining technique in machine learning has been proposed in [17]. Furthermore, a computationally efficient Legendre NN for nonlinear active noise cancellation is shown in [18].

The recurrent NN has received increasing attention due to its structural advantage in the modeling of the nonlinear system and dynamic control of the system [19-24]. These networks are capable of effective identification and control of complex process dynamics, but with the expense of large computational complexity. However, in the complicated nonlinear dynamic system such as PMSM servodrive electric scooter system, the flux linkage and external force interference is always an important factor. Hence, if each neuron in the recurrent neural networks is considered as a state in the nonlinear dynamic systems, the self-connection feedback type is unable to approximate the dynamic systems efficiently. In order to improve the ability of identifying high order systems, the modified recurrent Legendre NN has been proposed in this study. It has more advantages than the Legendre NN, including a better performance, higher accuracy, dynamic robustness, and a fast

transient performance.

Adaptive control algorithms are well developed for accurate control of robot manipulators under the presence of considerable uncertainty in the mass-related properties of the robot or its payload [25-26]. However, a critical assumption in these controllers is that the uncertain term should satisfy the linearity-in-parameters condition. Moreover, tedious analysis and computations have to be done to determine the regressor matrix. To overcome these drawbacks, a class of fuzzy-based and a class of neural-network-based adaptive approaches have been proposed for the manipulator tracking problem [27-32]. In [27], the tracking control of an electrically driven nonholonomic mobile robot with model uncertainties in the robot kinematics, the robot dynamics, and the wheel actuator dynamics is investigated. A robust adaptive controller is proposed with the utilization of adaptive control, backstepping and fuzzy logic techniques to raise robustness. In [28], the adaptive control of mobile robots via neural and wavelet networks is proposed to improve dynamic perform. In [29], an adaptive neural network algorithm is developed for rigid-link electrically-driven robot systems. An actual neural network controller is used to handle the uncertainty in the mechanical and electrical dynamics. In [30], a new robust output feedback control approach for flexible-joint electrically driven robots via the observer dynamic surface design technique is proposed to acquire good tracking performance using an adaptive observer with self-recurrent wavelet neural networks. In [31], a neural-network-based adaptive controller is proposed for the tracking problem of manipulators with uncertain kinematics, dynamics and actuator model. The adaptive Jacobian scheme is used to estimate the unknown kinematics parameters. Uncertainties in the manipulator dynamics and actuator model are compensated by three-layer neural networks. In [32] proposed an adaptive output-feedback control method based on neural networks for flexible link manipulator which is a nonlinear nonminimum phase system.

Owing to electric scooter with highly nonlinear dynamics [33-42], the many controllers may not provide satisfactory control performance when operated over a wide range of operating conditions. In [33-34], the hybrid recurrent fuzzy neural network (RFNN) control system is developed for PMSM driven wheel of electric scooter. The experimental results of control performance in the hybrid RFNN control system were only implemented under nominal condition and 4 times variations of rotor inertia and viscous friction with cycle variation of speed at 1200 rpm case. The favorable speed tracking responses can be only achieved under nominal case. The poor speed tracking responses are shown in experimental results under parameter variation at 1200 rpm case due to uncertain perturbations. Moreover, in order to reduce interference of encoder and cost down,

the hybrid RFNN control system using rotor flux estimator proposed by [35-37] was developed for controlling the PMSM driven electric scooter without shaft encoder. The rotor flux estimator consists of the estimation algorithm of rotor flux position and speed based on the back electromagnetic force (EMF) in order to supply with hybrid RFNN controller. In [35], the experimental results of control performance in the hybrid RFNN control system using rotor flux estimator were only implemented at two cases, i.e., 1200 rpm and 2400 rpm cases without adding and shedding load. In [36], the experimental results of control performance in the hybrid RFNN control system using rotor flux estimator were implemented at three cases, i.e., 1200 rpm case, 2400 rpm case and under external load torque 2 Nm with adding load and shedding load at 2400 rpm case. In [37], the comparative studies of control performances for the PI controller and the hybrid RFNN control system using rotor flux estimator were implemented at three cases, i.e., 1200 rpm case, 2400 rpm case and under external load torque 2 Nm with adding load and shedding load at 2400 rpm case. In addition, in [38], the hybrid recurrent NN (RNN) control system using rotor flux estimator is developed for PMSM driven wheel of electric scooter. The experimentation of the hybrid RNN control system using rotor flux estimator only were implemented at two cases, i.e., 1200 rpm case and 2400 rpm case without adding and shedding load. However, the better speed and current tracking responses are not shown in experimental results by using the above control methods due to no better nonlinear approximation ability under uncertain perturbations. Therefore, the hybrid recurrent wavelet NN (RWNN) control system using rotor flux estimator proposed by [39] is developed for PMSM driven electric scooter in order to acquire better control performance for nonlinear uncertainties. In [39], the comparative studies of control performances for the hybrid RFNN control system and the hybrid RWNN control system using rotor flux estimator were implemented at two cases, i.e., 1200 rpm case and 2400 rpm case. The speed and current tracking responses of the hybrid RWNN control system using rotor flux estimator have better performances than the hybrid RFNN control system from experimental results. Moreover, the hybrid RWNN control system proposed by [40-41] is developed for PMSM driven electric scooter in order to acquire better control performance for nonlinear uncertainties. In [40], the comparative studies of control performances for the hybrid RNN control system and the hybrid RWNN control system were implemented at two cases, i.e., 1200 rpm case and 2400 rpm case. In [41], the comparative studies of control performances for the PI control system and the hybrid RWNN control system were implemented at three cases, at three cases, i.e., 1200 rpm case, 2400 rpm case and under external load torque 2 Nm with adding load

and shedding load at 2400 rpm case. However, the speed and current tracking responses of the hybrid RWNN control system have better performances than the PI control system and the hybrid RNN control system from experimental results. Furthermore, the hybrid modified Elman NN control system was proposed by [42] in order to enhance nonlinear approximation capacity of RNN. In [42], the comparative studies of control performances for the PI control system and the hybrid modified Elman NN control system were implemented at three cases, at four cases, i.e., 1200 rpm case, 2400 rpm case, under external load torque 2 Nm and with adding load and shedding load at 2400 rpm case under external load torque 4 Nm and with adding load and shedding load at 2400 rpm are shown in experimental results. The tracking responses of speed and current of the hybrid modified Elman NN control system have better performances than the PI control system from experimental results. In addition, the load regulation of the hybrid modified Elman NN control system was better performance than the PI control system from experimental results. However, the used recurrent NNs with fixed learning rates of weights parameters in the above control methods have the slower convergence speed. Meanwhile, in order to ensure the control performance of robustness, the novel adaptive modified recurrent Legendre NN control system with two varied learning rates is developed for controlling the PMSM servo-drive electric scooter in this paper. The novel adaptive modified recurrent Legendre NN control system, which is composed of a modified recurrent Legendre NN control with adaptation law and a remunerated control with estimation law, is applied to PMSM servo-drive electric scooter system. The novel adaptive modified recurrent Legendre NN control system has fast convergence ability and good generalization capability. In addition, the online parameter adaptation law of the modified recurrent Legendre NN and the estimation law of the remunerated controller can be derived according to Lyapunov stability theorem and gradient descent method. Furthermore, the modified recurrent Legendre NN with two variable learning rates is proposed to raise convergence speed. The control method, which is not dependent upon the predetermined characteristics of the system owing to the online learning ability being able to capture the system's nonlinear and time-varying behaviors, can adapt to any change in the system characteristics. Finally, the control performance of the proposed novel adaptive modified recurrent Legendre NN control system is verified by experimental results.

The remainder of this paper is organized as follows: The configuration of Pmsm servo-drive electric scooter system is reviewed in Section 2. A design method of novel adaptive modified recurrent Legendre NN control system is presented in Section 3. Experimental results are illus-

trated in Section 4. Some conclusions are given in Section 5.

## 2 STRUCTURE OF PMSM SERVO-DRIVE ELECTRIC SCOOTER SYSTEM

The  $d$ -axis and  $q$ -axis voltage equations of the PMSM servo-drive electric scooter in the rotating reference frame can be described as following as [1-3]:

$$v_{qr} = R_r i_{qr} + L_{qr} p i_{qr} + P_r \omega_c (L_{dr} i_{dr} + \lambda_{fd}) / 2 \quad (1)$$

$$v_{dr} = R_r i_{dr} + L_{dr} p i_{dr} - P_r \omega_c L_{qr} i_{qr} / 2 \quad (2)$$

in which  $v_{qr}$  and  $v_{dr}$  are the  $d$ -axis and  $q$ -axis voltages,  $i_{qr}$  and  $i_{dr}$  are the  $d$ -axis and  $q$ -axis currents,  $L_{qr}$  and  $L_{dr}$  are the  $d$ -axis and  $q$ -axis inductances,  $\lambda_{fd}$  is the  $d$ -axis permanent magnet flux linkage,  $R_r$  is the stator resistance,  $P_r$  is the number of poles,  $\omega_c = 2\omega_f / P_r$  is the rotor speed,  $\omega_f$  is the electrical angular frequency,  $p = d/dt$  is a differential operator. The electromagnetic torque  $T_e$  of a PMSM servo-drive electric scooter can be described as

$$T_e = 3P_r [\lambda_{fd} i_{qr} + (L_{dr} - L_{qr}) i_{dr} i_{qr}] / 4 \quad (3)$$

Then the dynamic equation of PMSM servo-drive electric scooter [33-44] can be represented as

$$J_r \dot{\omega}_c + B_r \omega_c = T_e - T_l(F_l, v_a, \tau_a, \omega_c^2) \quad (4)$$

in which  $T_l(F_l, v_a, \tau_a, \omega_c^2)$  is the lumped nonlinear external disturbance, e.g. electric scooter system (including the rolling resistance  $v_a$ , wind resistance  $\tau_a$  and braking force  $F_l$ ),  $B_r$  represents the total viscous frictional coefficient and  $J_r$  is the total moment of inertia including electric scooter. The pulse width modulation (PWM) control principle of the PMSM servo-drive system is based on field orientation. Due to  $L_{dr} = L_{qr}$  and  $i_{dr} = 0$  for the surface-mounted PMSM, the second term of (3) is zero. In addition,  $\lambda_{fd}$  is a constant for a field-oriented control of surface-mounted PMSM, thus, the electromagnetic torque  $T_e$  is linearly proportional to the  $q$ -axis current  $i_{qr}$ . Therefore the  $d$ -axis rotor flux is a constant, the maximum torque per ampere can be reached under the field-oriented control. The PMSM servo-drive system with the implementation of field-oriented control can be reduced as

$$T_e = k_r i_{qr}^* \quad (5)$$

in which  $k_r = 3P_r \lambda_{fd} / 4$  is the torque constant. The block diagram of whole system for a PMSM servo-drive electric scooter is shown in Fig. 1.

Figure 1 indicated as follows: a field orientation institution, a proportional integral derivative (PID) current control loop, a sinusoidal PWM control circuit, an interlock circuit and an isolated circuit, an insulated gate bipolar transistor (IGBT) power module inverter and a speed control loop. The PID current controller is the current loop tracking controller. In order to attain good dynamic response, all control gains for PID current loop controller are listed as follows:  $k_{pc} = 8$ ,  $k_{ic} = 2.5$  and  $k_{dc} = 0.5$ . The field orientation institution makes up coordinate transformation,  $\sin \theta_f / \cos \theta_f$  generation and lookup table generation. The TMS320C32 DSP control system is used to implement field orientation institution and speed control. The PMSM servo-drive electric scooter is manipulated at load disturbance torque with nonlinear uncertainties.

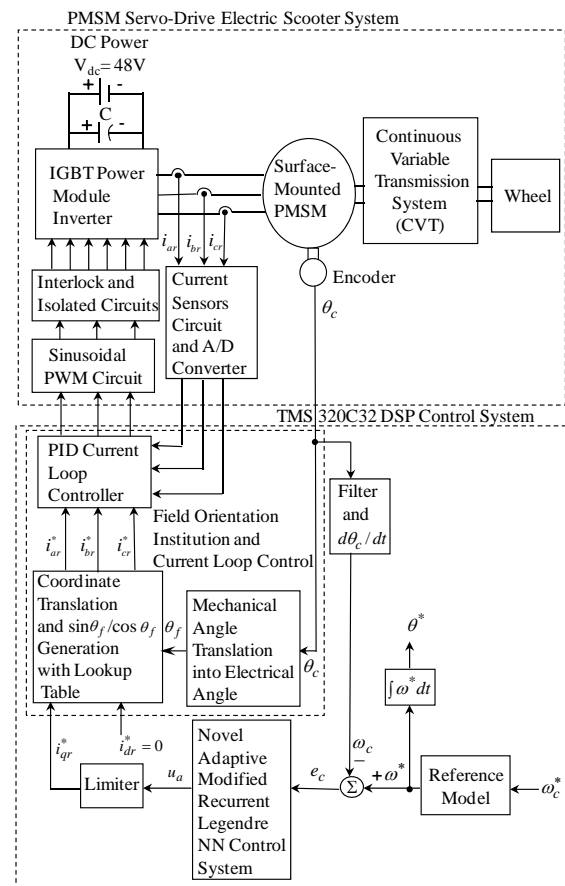


Fig. 1. Block diagram of a PMSM servo-drive electric scooter system

### 3 DESIGN OF NOVEL ADAPTIVE MODIFIED RECURRENT LEGENDRE NN CONTROL SYSTEM

Owing to nonlinear uncertainties of the electric scooter such as nonlinear friction force of the transmission belt and clutch, these will lead to degenerate tracking responses in command current and speed of the PMSM servo-drive electric scooter. The variation of rotor inertia and friction of PMSM servo-drive electric scooter cause nonlinear uncertainties. These uncertainties are difficult to establish exact models. Therefore, for convenient design of the novel adaptive modified recurrent Legendre NN control system, the dynamic equation of the PMSM servo-drive electric scooter from (4) can be rewritten as

$$\begin{aligned} \dot{\omega}_c &= -B_r\omega_c/J_r - T_l(F_l, v_a, \tau_a, \omega_c^2)/J_r + k_r i_{qr}^*/J_r \\ &= A_a\omega_c + C_a T_l(F_l, v_a, \tau_a, \omega_c^2) + B_a u_a \end{aligned} \tag{6}$$

in which  $u_a = i_{qr}^*$  is the  $q$ -axis command current of the PMSM.  $A_a = -B_r/J_r$ ,  $B_a = k_r/J_r$ , and  $C_a = -1/J_r$  are three known constants. When the uncertainties including variation of system parameters and external force disturbance occur, the parameters are assumed to be bounded, i.e.,  $|A_a\omega_c| \leq D_1(\omega_c)$ ,  $|C_a T_l(F_l, v_a, \tau_a, \omega_c^2)| \leq D_2$  and  $D_3 \leq B_a$ , where  $D_1(\omega_c)$  is a known continuous function,  $D_2$  and  $D_3$  are two bounded constants. Then, the tracking error can be defined as

$$e_c = \omega^* - \omega_c \tag{7}$$

where  $\omega^*$  represents the desired command rotor speed,  $e_c$  is the tracking error between the desired rotor speed and rotor speed. If all parameters of the PMSM servo-drive system including external load disturbance are well known, the ideal control law can be designed as

$$u_a^* = [\dot{\omega}^* + k_1 e_c - A_a\omega_c - C_a T_l(F_l, v_a, \tau_a, \omega_c^2)]/B_a \tag{8}$$

in which  $k_1 > 0$  is a constant. Replace (8) of (6), the error dynamic equation can be obtained

$$\dot{e}_c + k_1 e_c = 0 \tag{9}$$

The system state can track the desired trajectory gradually if  $e_c(t) \rightarrow 0$  as  $t \rightarrow \infty$  in (9). However, the novel adaptive recurrent Legendre NN control system is proposed to control PMSM servo-drive electric scooter under uncertainty perturbation. The configuration of the proposed novel adaptive modified recurrent Legendre NN control system is described in Fig. 2.

The novel adaptive modified recurrent Legendre NN control system composed of a modified recurrent Legendre NN controller with adaptation law and a remunerated controller with estimation law. The control law is designed as

$$u_a = u_{re} + u_{rc} \tag{10}$$

where  $u_{re}$  is the modified recurrent Legendre NN control which is as the major tracking controller. It is used to imitate an ideal control law. The remunerated control  $u_{rc}$  is designed to remunerate the difference between the ideal control law and the modified recurrent Legendre NN control. An error dynamic equation from (6) to (10) can be acquired as

$$\dot{e}_c = -k_1 e_c + [u_a^* - u_{re} - u_{rc}]B_a \tag{11}$$

The modified recurrent Legendre NN control and remunerated control can be devised to conquer the mentioned blemish. The modified recurrent Legendre NN control raised to imitate the ideal control  $u_a^*$ . Then a remunerated control posed to remunerate the difference between ideal control  $u_a^*$  and the modified recurrent Legendre NN control  $u_{re}$ .

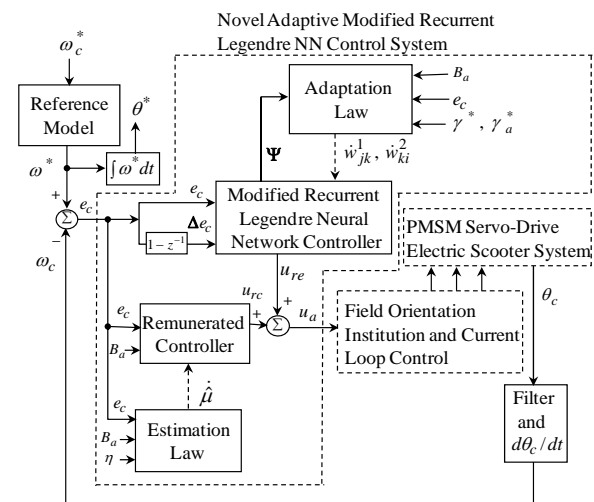


Fig. 2. Block diagram of the novel adaptive modified recurrent Legendre NN control system

Firstly, the architecture of the proposed three-layer modified recurrent Legendre NN is depicted in Fig. 3. It is composed of an input layer, a hidden layer and an output layer. The activation functions and signal actions of nodes in each layer of the modified recurrent Legendre NN can be described as follows:

*First layer: input layer*

Each node  $i$  in this layer is indicated by using  $\Pi$ , which multiplies by each other between each other for input signals. Then outputs signals are the results of product. The input and the output for each node  $i$  in this layer are expressed as

$$\begin{aligned} nod_i^1 &= \prod_k x_i^1(N)w_{ki}^2y_k^3(N-1), \\ y_i^1 &= f_i^1(nod_i^1) = nod_i^1, \quad i = 1, 2 \end{aligned} \tag{12}$$

The  $x_1^1 = \omega^* - \omega_c = e_c$  is the tracking error between the desired speed  $\omega^*$  and the rotor speed  $\omega_c$ . The  $x_2^1 = e_c(1 - z^{-1}) = \Delta e_c$  is the tracking error change. The  $w_{ki}^2$  is the recurrent weight between output layer and input layer. The  $N$  denotes the number of iterations. The  $y_k^3$  is the output value of the output layer in the modified recurrent Legendre NN.

*Second layer: hidden layer*

The single node  $j$ th in this layer is labeled with  $\Sigma$ . The net input and the net output for node  $j$ th of the hidden layer are expressed as

$$nod_j^2 = \sum_{i=1}^2 y_i^1, \quad y_j^2 = f_j^2(L_j(nod_j^2)), \quad j = 0, 1, \dots, m-1 \tag{13}$$

Legendre polynomials [14-16] are selected for activation function of the hidden layer. The Legendre polynomials are denoted by  $L_n(x)$ , where  $n$  is the order of expansion and  $-1 < x < 1$  is the argument of the polynomial,  $m$  is the number of nodes. The zero, the first and the second order Legendre polynomials are given by  $L_0(x) = 1$ ,  $L_1(x) = x$  and  $L_2(x) = (3x^2 - 1)/2$ , respectively. The higher order polynomials are given by  $L_3(x) = (5x^3 - 3x)/2$  and  $L_4(x) = (35x^4 - 30x^2 + 3)/8$ . The higher order Legendre polynomials may be generated by the recursive formula given by  $L_{n+1}(x) = [(2n + 1)xL_n(x) - nL_{n-1}(x)]/(n + 1)$ .

*Third layer: output layer*

The single node  $k$ th in this layer is labeled with  $\Sigma$ . It computes the overall output as the summation of all input signals. The net input and the net output for node  $k$ th in this layer are expressed as

$$\begin{aligned} nod_k^3 &= \sum_{j=0}^{m-1} w_{jk}^1 y_j^2(N), \\ y_k^3 &= f_k^3(nod_k^3) = nod_k^3, \quad k = 1 \end{aligned} \tag{14}$$

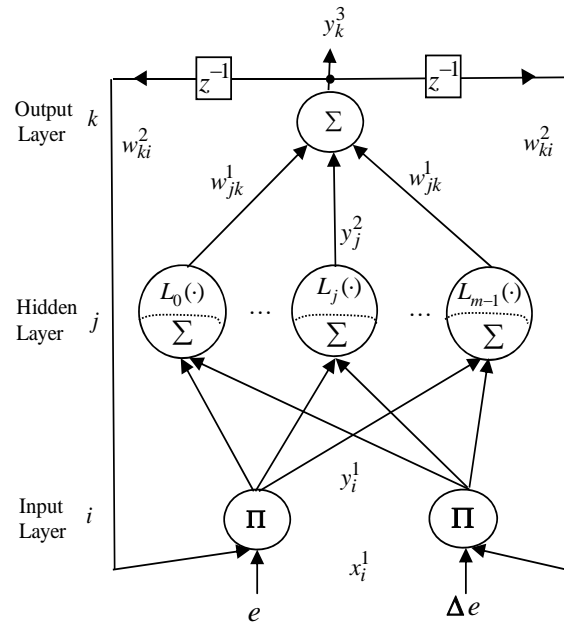


Fig. 3. Structure of the three-layer modified recurrent Legendre NN

where  $w_{jk}^1$  is the connective weight between the hidden layer and the output layer;  $f_k^3$  is the activation function, which is selected as a linear function;  $x_k^3(N) = y_j^2(N)$  represents the  $j$ th input to the node of output layer. The output value of the modified recurrent Legendre NN can be represented as  $y_k^3(N) = u_{re}$ . Then the output value of the modified recurrent Legendre NN,  $u_{re}$ , can be denoted as

$$u_{re} = \Theta^T \Psi \tag{15}$$

in which  $\Theta = [w_{01}^1 \dots w_{m-1,1}^1]^T$  is the adjustable weight parameters vector between the hidden layer and the output layer of the recurrent Legendre NN.  $\Psi = [x_0^3 \dots x_{m-1}^3]^T$  is the inputs vector in the output layer of the modified recurrent Legendre NN, in which  $x_j^3$  is determined by the selected Legendre polynomials.

Secondly, in order to evolve the remunerated control  $u_{re}$ , a minimum affinity error  $\sigma$  is defined as

$$\sigma = u_a^* - u_{re}^* = u_a^* - (\Theta^*)^T \Psi \tag{16}$$

in which  $\Theta^*$  is an ideal weight vector to reach of minimum affinity error. It is assumed that absolute value of  $\sigma$  is less than a small positive constant  $\mu$ , i.e.,  $|\sigma| < \mu$ . Then, the

error dynamic equation from (11) can be rewritten as

$$\begin{aligned} \dot{e}_c &= -k_1 e_c + [(u_a^* - u_{re}) - u_{rc}] B_a \\ &= -k_1 e_c + [(u_a^* - u_{re}^* + u_{re}^* - u_{re}) - u_{rc}] B_a \\ &= -k_1 e_c + [(u_a^* - u_{re}^*) + (\Theta^*)^T \Psi - (\Theta)^T \Psi - u_{rc}] B_a \\ &= -k_1 e_c + [\sigma + (\Theta^* - \Theta)^T \Psi - u_{rc}] B_a \end{aligned} \tag{17}$$

Then, the Lyapunov function is selected as

$$v_1(t) = e_c^2/2 + (\Theta^* - \Theta)^T (\Theta^* - \Theta) / (2\gamma) + \tilde{\mu}^2 / (2\eta) \tag{18}$$

in which  $\gamma$  is a learning rate;  $\eta$  is an adaptation gain;  $\tilde{\mu} = \hat{\mu} - \mu$  is the bound estimated error. Differentiating the Lyapunov function with respect to  $t$  and using (17), then (18) can be rewritten as

$$\begin{aligned} \dot{v}_1(t) &= \dot{e}_c e_c - (\Theta^* - \Theta)^T \dot{\Theta} / \gamma + \tilde{\mu} \dot{\mu} / \eta \\ &= \{-k_1 e_c^2 + [\sigma - u_{rc}] B_a\} e_c + \tilde{\mu} \dot{\mu} / \eta \\ &\quad + (\Theta^* - \Theta)^T \Psi B_a e_c - (\Theta^* - \Theta)^T \dot{\Theta} / \gamma \end{aligned} \tag{19}$$

In order to  $\dot{v}_1 \leq 0$ , the adaptation law  $\dot{\Theta}$ , the remunerated controller  $u_{rc}$  with estimation law can be designed as follow as

$$\dot{\Theta} = \gamma \Psi B_a e_c \tag{20}$$

$$u_{rc} = \hat{\mu} \text{sgn}(B_a e_c) \tag{21}$$

$$\dot{\hat{\mu}} = \eta |B_a e_c| \tag{22}$$

In order to avoid chattering phenomenon of sliding mode, the sign function  $\text{sgn}(B_a e_c)$  can be replaced by the equation  $B_a e_c / (|B_a e_c| + \rho)$ , where  $\rho = \begin{cases} \rho_0, & |B_a e_c| < \varepsilon \\ 0, & |B_a e_c| \geq \varepsilon \end{cases}$  and  $\rho_0$  and  $\varepsilon$  are two positive constants. Substituting (20) into (19), then (19) can be represented as

$$\dot{v}_1(t) = -k_1 e_c^2 + \{\sigma - u_{rc}\} B_a e_c + \tilde{\mu} \dot{\mu} / \eta \tag{23}$$

Substituting (21) and (22) into (23), then (23) can be obtained as

$$\begin{aligned} \dot{v}_1(t) &= -k_1 e_c^2 + \{\sigma - \hat{\mu} \text{sgn}(B_a e)\} B_a e_c \\ &\quad + (\hat{\mu} - \mu) (\eta |B_a e_c|) / \eta \\ &\leq -k_1 e_c^2 + \{|\sigma| - \hat{\mu}\} |B_a e_c| + (\hat{\mu} - \mu) |B_a e_c| \\ &= -k_1 e_c^2 + \{|\sigma| - \mu\} |B_a e_c| \\ &\leq -k_1 e_c^2 \\ &\leq 0 \end{aligned} \tag{24}$$

From (24), the  $\dot{v}_1(t)$  is a negative semi-definite function, i.e.,  $v_1(t) \leq v_1(0)$ . It implies that  $e_c$  and  $(\Theta^* - \Theta)$  be bounded. For the sake of proof of the proposed novel adaptive modified recurrent Legendre NN control system to be gradually stable, the function is defined as

$$\phi(t) = -\dot{v}_1(t) = k_1 e_c^2 \tag{25}$$

Integrating (25) with respect to  $t$ , then

$$\int_0^t \phi(\tau) d\tau = \int_0^t [-\dot{v}_1(t)] dt = v_1(0) - v_1(t) \tag{26}$$

Owing to  $v_1(0)$  is bounded, and  $v_1(t)$  is a nonincreasing and bounded function, then

$$\lim_{t \rightarrow \infty} \int_0^t \phi(\tau) d\tau < \infty \tag{27}$$

Differentiating (25) with respect to  $t$  gives

$$\dot{\phi}(t) = 2k_1 e_c \dot{e}_c \tag{28}$$

Owing to all the variables in the right side of (17) are bounded. It implies that  $\dot{e}_c$  is also bounded. Then,  $\phi(t)$  is a uniformly continuous function [45-46]. It is denoted that  $\lim_{t \rightarrow \infty} \phi(t) = 0$  by using Barbalat's lemma [45-46], i.e.,  $e_c(t) \rightarrow 0$  as  $t \rightarrow \infty$ . Therefore, the novel adaptive modified recurrent Legendre NN control system is gradually stable from proof. Moreover, the tracking error  $e_c(t)$  of the system will converge to zero.

According to Lyapunov stability theorem and the gradient descent method, an online parameter tuning methodology of the modified recurrent Legendre NN can be derived and tuned effectively. The parameters of adaptation law  $\dot{\Theta}$  can be computed by the gradient descent method and the chain rule. The adaptation law  $\dot{\Theta}$  shown in (20) calls for a proper choice of the learning rate. For a small value of learning rate, the convergence of controller parameter can be guaranteed but the convergent speed is very slow. On the other hand, if the learning-rate is too large, the parameter convergence may become more unstable. In order to train the modified recurrent Legendre NN efficiently, an optimal learning rate will be derived to achieve the fast convergence of output tracking error. Firstly, the adaptation law  $\dot{\Theta}$  shown in (20) can be rewritten as

$$\dot{w}_{jk}^1 = \gamma x_j^3 B_a e_c \tag{29}$$

The central part of the tuning algorithm for the modified recurrent Legendre NN concerns how to obtain recursively a gradient vector in which each element in the tuning

algorithm is defined as the derivative of an energy function with respect to a parameter of the network. This is done by means of the chain rule, because the gradient vector is calculated in the direction opposite to the flow of the output of each node. In order to describe the online tuning algorithm of the modified recurrent Legendre NN, a cost function is defined as

$$V_1 = e_c^2/2 \tag{30}$$

According to the gradient descent method, the adaptation law of the weight between the hidden layer and the output layer also can be represented as

$$\begin{aligned} \dot{w}_{jk}^1 &= -\gamma \frac{\partial V_1}{\partial w_{jk}^1} \\ &= -\gamma \frac{\partial V_1}{\partial u_{re}} \frac{\partial u_{re}}{\partial y_k^3} \frac{\partial y_k^3}{\partial nod_k^3} \frac{\partial nod_k^3}{\partial w_{jk}^1} = -\gamma \frac{\partial V_1}{\partial y_k^3} x_j^3 \end{aligned} \tag{31}$$

Comparing (29) with (31), yields  $\partial V_1/\partial y_k^3 = -B_a e_c$ .

The adaptation law of recurrent weight  $w_{ki}^2$  using the gradient descent method can be updated as

$$\begin{aligned} \dot{w}_{ki}^2 &= -\gamma_a \frac{\partial V_1}{\partial u_{re}} \frac{\partial u_{re}}{\partial y_k^3} \frac{\partial y_k^3}{\partial y_j^2} \frac{\partial y_j^2}{\partial nod_j^2} \frac{\partial nod_j^2}{\partial y_i^1} \frac{\partial y_i^1}{\partial nod_i^1} \frac{\partial nod_i^1}{\partial w_{ki}^2} \\ &= \gamma_a B_a e_c w_{jk}^1 L_j(\cdot) x_i^1(N) y_k^3(N-1) \end{aligned} \tag{32}$$

in which  $\gamma_a$  is a learning rate. Then, the convergence analysis in the following theorem is to derive specific learning rate to assure convergence of the output tracking error.

**Theorem 1:** Let  $\gamma$  be the learning rate of the modified recurrent Legendre NN weights between the hidden layer and the output layer, and let  $P_{1w \max}$  be defined as  $P_{1w \max} \equiv \max_N \|P_{1w}(N)\|$ , where  $P_{1w}(N) = \partial y_k^3/\partial w_{jk}^1$  and  $\|\cdot\|$  is the Euclidean norm in  $\mathbb{R}^n$ . Then, the convergence of the output tracking error is guaranteed if is chosen as

$$0 < \gamma < \frac{2}{(P_{1w \max})^2 [B_a e_c/e_c(N)]^2} \tag{33}$$

Moreover, the optimal learning rate which achieves the fast convergence can be obtained as

$$\gamma^* = 1/[(P_{1w \max})^2 [B_a e_c/e_c(N)]^2] \tag{34}$$

**Proof:** Since

$$P_{1w}(N) = \frac{\partial y_k^3}{\partial w_{jk}^1} = x_j^3 \tag{35}$$

Then, a discrete-type Lyapunov function is selected as

$$L_2(N) = \frac{1}{2} e_c^2(N) \tag{36}$$

The change in the Lyapunov function is obtained by

$$\begin{aligned} \Delta L_2(N) &= L_2(N+1) - L_2(N) \\ &= \frac{1}{2} [e_c^2(N+1) - e_c^2(N)] \end{aligned} \tag{37}$$

The error difference can be represented by

$$\begin{aligned} e_c(N+1) &= e_c(N) + \Delta e_c(N) \\ &= e_c(N) + \left[ \frac{\partial e_c(N)}{\partial w_{jk}^1} \right]^T \Delta w_{jk}^1 \end{aligned} \tag{38}$$

where  $\Delta e_c(N)$  is the output error change  $\Delta w_{jk}^1$  represents change of the weight. Using (29), (30), (31) and (35), then (38) can be obtained

$$\frac{\partial e_c(N)}{\partial w_{jk}^1} = \frac{\partial e_c(N)}{\partial V_1} \frac{\partial V_1}{\partial y_k^3} \frac{\partial y_k^3}{\partial w_{jk}^1} = -\frac{B_a e_c}{e_c(N)} P_{1w}(N) \tag{39}$$

$$e_c(N+1) = e_c(N) - \left[ \frac{B_a e_c}{e_c(N)} P_{1w}(N) \right]^T \gamma B_a e_c P_{1w}(N) \tag{40}$$

Thus

$$\begin{aligned} \|e_c(N+1)\| &= \|e_c(N) \\ &\cdot [1 - \gamma (B_a e_c/e_c(N))^2 P_{1w}^T(N) P_{1w}(N)]\| \\ &\leq \|e_c(N)\| \|1 - \gamma (B_a e_c/e_c(N))^2 P_{1w}^T(N) P_{1w}(N)\| \end{aligned} \tag{41}$$

From (37) to (41),  $\Delta L_2(N)$  can be rewritten as

$$\begin{aligned} \Delta L_2(N) &= \frac{1}{2} \gamma [B_a e_c]^2 P_{1w}^T(N) P_{1w}(N) \\ &\cdot \left\{ \gamma [B_a e_c/e_c(N)]^2 P_{1w}^T(N) P_{1w}(N) - 2 \right\} \\ &\leq \frac{1}{2} \gamma [B_a e_c]^2 (P_{1w \max}(N))^2 \\ &\cdot \left\{ \gamma [B_a e_c/e_c(N)]^2 (P_{1w \max}(N))^2 - 2 \right\} \end{aligned} \tag{42}$$

If  $\gamma$  is chosen as  $0 < \gamma < 2/\{(P_{1w \max})^2 [B_a e_c/e_c(N)]^2\}$ , then the Lyapunov stability of  $L_2(N) > 0$  and  $\Delta L_2(N) < 0$  is guaranteed so that the output tracking error will converge to zero as  $t \rightarrow \infty$ . This completes the proof of the theorem. Moreover, the optimal learning-rate which achieves the fast convergence is corresponding to

$$2\gamma^* \{(P_{1w \max})^2 [B_a e_c / e_c(N)]^2\} - 2 = 0 \quad (43)$$

i.e.,

$$\gamma^* = 1 / \{(P_{1w \max})^2 [B_a e_c / e_c(N)]^2\} \quad (44)$$

which comes from the derivative of (42) with respect to  $\gamma$  and equals to zero. This shows an interesting result for the variable optimal learning rate which can be online tuned at each instant. In summary, the online learning algorithm of the modified recurrent Legendre NN controller is based on the adaptation law (29) for the weight adjustment with the optimal learning rate in (34).

**Theorem 2:** Let  $\gamma_a$  be the learning rate of the modified recurrent Legendre NN weights between the output layer and the input layer, and let  $P_{2w \max}$  be defined as  $P_{2w \max} \equiv \max_N \|P_{2w}(N)\|$ , where  $P_{2w}(N) = \partial y_k^3 / \partial w_{ki}^2$  and  $\|\cdot\|$  is the Euclidean norm in  $\mathbb{R}^n$ . Then, the convergence of the output tracking error is guaranteed if is chosen as

$$0 < \gamma_a < \frac{2}{(P_{2w \max})^2 [B_a e_c / e_c(N)]^2} \quad (45)$$

Moreover, the optimal learning rate which achieves the fast convergence can be obtained as

$$\gamma_a^* = 1 / \{(P_{2w \max})^2 [B_a e_c / e_c(N)]^2\} \quad (46)$$

**Proof:** Since

$$P_{2w}(N) = \frac{\partial y_k^3}{\partial w_{ki}^2} = w_{jk}^1 L_j(\cdot) x_i^1(N) y_k^3(N-1) \quad (47)$$

Then, a discrete-type Lyapunov function is selected as (36) and the change in the Lyapunov function is obtained by (37).

The error difference can be represented by

$$\begin{aligned} e_c(N+1) &= e_c(N) + \Delta e_c(N) \\ &= e_c(N) + \left[ \frac{\partial e_c(N)}{\partial w_{ki}^2} \right]^T \Delta w_{ki}^2 \end{aligned} \quad (48)$$

where  $\Delta e_c(N)$  is the output error change  $\Delta w_{ki}^2$  represents change of the weight. Using (30), (32) and (47), then (48) can be obtained

$$\begin{aligned} \frac{\partial e_c(N)}{\partial w_{ki}^2} &= \frac{\partial e_c(N)}{\partial V_1} \frac{\partial V_1}{\partial y_k^3} \frac{\partial y_k^3}{\partial w_{ki}^2} \\ &= -\frac{B_a e_c}{e_c(N)} P_{2w}(N) \end{aligned} \quad (49)$$

$$e_c(N+1) = e_c(N)$$

$$- \left[ \frac{B_a e_c}{e_c(N)} P_{2w}(N) \right]^T \gamma_a B_a e_c P_{2w}(N) \quad (50)$$

Thus

$$\begin{aligned} \|e_c(N+1)\| &= \\ \|e_c(N) \left[ 1 - \gamma_a (B_a e_c / e_c(N))^2 P_{2w}^T(N) P_{2w}(N) \right]\| & \\ \leq \|e_c(N)\| & \\ \cdot \left\| 1 - \gamma_a (B_a e_c / e_c(N))^2 P_{2w}^T(N) P_{2w}(N) \right\| & \end{aligned} \quad (51)$$

From (37), (49) to (51),  $\Delta L_2(N)$  can be rewritten as

$$\begin{aligned} \Delta L_2(N) &= \frac{1}{2} \gamma_a [B_a e_c]^2 P_{2w}^T(N) P_{2w}(N) \\ \cdot \left\{ \gamma_a [B_a e_c / e_c(N)]^2 P_{2w}^T(N) P_{2w}(N) - 2 \right\} & \\ \leq \frac{1}{2} \gamma_a [B_a e_c]^2 (P_{2w \max}(N))^2 & \\ \cdot \left\{ \gamma_a [B_a e_c / e_c(N)]^2 (P_{2w \max}(N))^2 - 2 \right\} & \end{aligned} \quad (52)$$

If  $\gamma_a$  is chosen as  $0 < \gamma_a < 2 / \{(P_{2w \max})^2 [B_a e_c / e_c(N)]^2\}$ , then the Lyapunov stability of  $L_2(N) > 0$  and  $\Delta L_2(N) < 0$  is guaranteed so that the output tracking error will converge to zero as  $t \rightarrow \infty$ . This completes the proof of the theorem. Moreover, the optimal learning-rate which achieves the fast convergence is corresponding to

$$2\gamma_a^* \{(P_{2w \max})^2 [B_a e_c / e_c(N)]^2\} - 2 = 0 \quad (53)$$

i.e.,

$$\gamma_a^* = 1 / \{(P_{2w \max})^2 [B_a e_c / e_c(N)]^2\} \quad (54)$$

which comes from the derivative of (52) with respect to  $\gamma_a$  and equals to zero. This shows an interesting result for the variable optimal learning rate which can be online tuned at each instant. In summary, the online learning algorithm of the modified recurrent Legendre NN controller is based on the adaptation law (32) for the weight adjustment with the optimal learning rate in (46).

#### 4 EXPERIMENTAL RESULTS

The whole system of the DSP-based control system for a PMSM servo-drive electric scooter system is shown in Fig. 1. A photo of the experimental setup is shown in Fig. 4. The control algorithm was executed by a TMS320C32

DSP control system includes 4-channels of D/A, 8-channels of programmable PWM and an encoder interface circuit. The IGBT power module voltage source inverter is executed by PID current-controlled SPWM with a switching frequency of 15 kHz. The specification of the used PMSM is 3-phase 48 V, 750 W, 3600 rpm. The parameters of the PMSM are given as  $\bar{J}_r = 62.15 \times 10^{-3} \text{ Nm}\cdot\text{s}$ ,  $\bar{B}_r = 6.18 \times 10^{-3} \text{ Nm}\cdot\text{s}/\text{rad}$ ,  $R_r = 2.5 \Omega$ ,  $L_{dr} = L_{qr} = 6.53 \text{ mH}$ ,  $k_r = 0.86 \text{ Nm}/\text{A}$  by means of open circuit test, short test, rotor block test, loading test.

The compared results of the control performance for a PMSM servo-drive electric scooter controlled using four kinds of control methods are shown by experimental tests. The proposed novel adaptive modified recurrent Legendre NN control system not only compared with two baseline controllers, i.e., the PI and PID controllers but also compared with a three-layer feedforward NN control system using sigmoid activation function in the hidden layer. All the parameters and the neurons of the novel modified recurrent Legendre NN control system are chosen to achieve the better transient performance and faster convergence in experimentation considering the requirement of stability. In this paper, the modified recurrent Legendre NN has two neurons, three neurons and one neuron in the input layer, the hidden layer and the output layer, respectively. The initialization of the modified recurrent Legendre NN parameters described in Refs. [15, 17] is adopted to initialize the parameters of the Legendre polynomial functions in this paper. The effect due to inaccurate selection of the initialized parameters can be retrieved by the online parameter training methodology. The parameter adjustment process remains continually active for the duration of the experimentation.

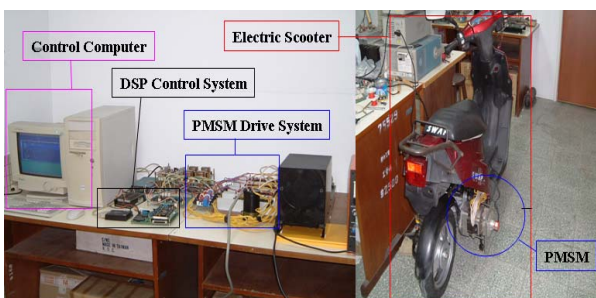


Fig. 4. A photo of the experimental setup

The PI control method, the PID control method, the three-layer feedforward NN control method and the novel adaptive modified recurrent Legendre NN control method are tested via two cases in the experimentation here, one being the 125.6 rad/s case, another being 251.2 rad/s case. All gains of the PI controller for the speed tracking are ob-

tained by trial and error method. In order to achieve good transient and steady-state control performance, all gains of the PI controller are  $k_{ps} = 16$  and  $k_{is} = 4$  through some heuristic knowledge [47-49] the gains of the PI controller on the tuning of the PI controller at the 125.6 rad/s case for the speed tracking. The speed tracking response of the rotor speed command  $\omega_c^*$ , the desired rotor speed command  $\omega^*$  and the measured rotor speed  $\omega_c$  for a PMSM servo-drive electric scooter using the PI controller at 125.6 rad/s case is shown in Fig. 5. The zoom error of speed response for a PMSM servo-drive electric scooter using the PI controller at 125.6 rad/s is shown in Fig. 6. The current tracking response of the command current  $i_{ar}^*$  and measured current  $i_{ar}$  in phase *a* for a PMSM servo-drive electric scooter using the PI controller at 125.6 rad/s case is shown in Fig. 7. The control effort  $u_a$  response for a PMSM servo-drive electric scooter using the PI controller at 125.6 rad/s case is shown in Fig. 8. The speed tracking response of the rotor speed command  $\omega_c^*$ , the desired rotor speed command  $\omega^*$  and the measured rotor speed  $\omega_c$  for a PMSM servo-drive electric scooter using the PI controller at 251.2 rad/s case is shown in Fig. 9. The zoom error of speed response for a PMSM servo-drive electric scooter using the PI controller at 251.2 rad/s is shown in Fig. 10. The current tracking response of the command current  $i_{ar}^*$  and measured current  $i_{ar}$  in phase *a* for a PMSM servo-drive electric scooter using the PI controller at 251.2 rad/s case is shown in Fig. 11. The control effort  $u_a$  response for a PMSM servo-drive electric scooter using the PI controller at 251.2 rad/s case is shown in Fig. 12.

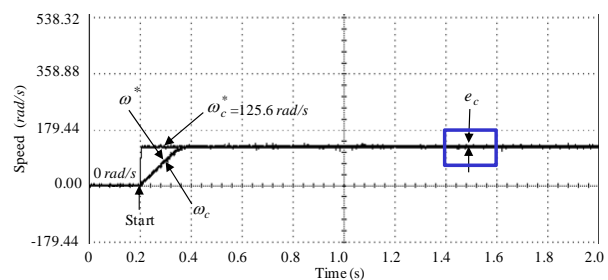


Fig. 5. Experimental result of the PI controller for a PMSM servo-drive electric scooter at 125.6 rad/s case with speed tracking response

In addition, all gains of the PID controller, which is listed as  $k_{ps} = 16.5$ ,  $k_{is} = 4.5$  and  $k_{ds} = 1.2$  at the 125.6 rad/s case for the speed tracking through some heuristic knowledge [47-49] the gains of the PID controller on the tuning of the PID controller in order to achieve good transient and steady-state control performance. The speed tracking response of the rotor speed command  $\omega_c^*$ , the

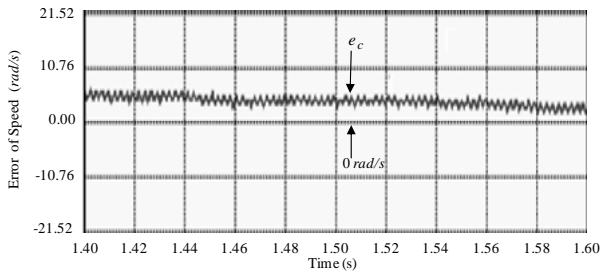


Fig. 6. Experimental result of the PI controller for a PMSM servo-drive electric scooter at 125.6 rad/s case with zoom error of speed response

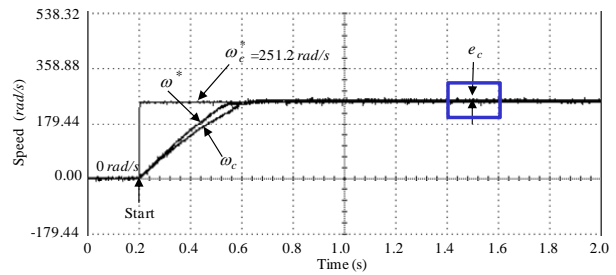


Fig. 9. Experimental result of the PI controller for a PMSM servo-drive electric scooter at 251.2 rad/s case with speed tracking response

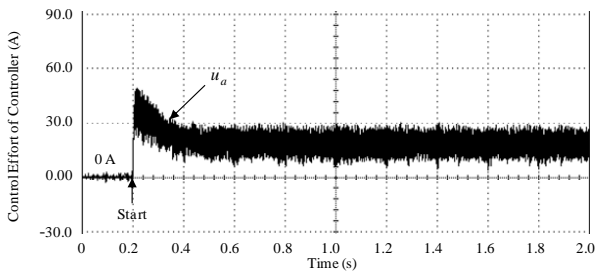


Fig. 7. Experimental result of the PI controller for a PMSM servo-drive electric scooter at 125.6 rad/s case with control effort response

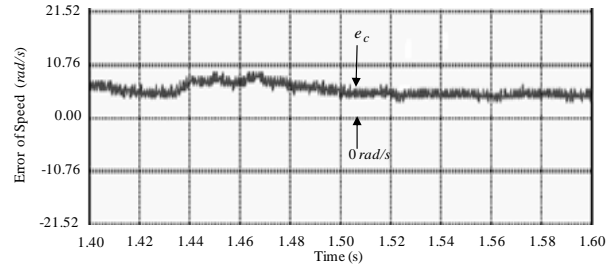


Fig. 10. Experimental result of the PI controller for a PMSM servo-drive electric scooter at 251.2 rad/s case with zoom error of speed response

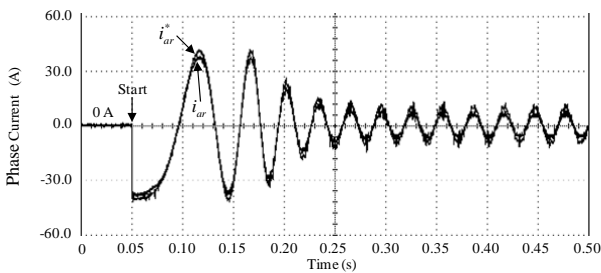


Fig. 8. Experimental result of the PI controller for a PMSM servo-drive electric scooter at 125.6 rad/s case with current tracking response

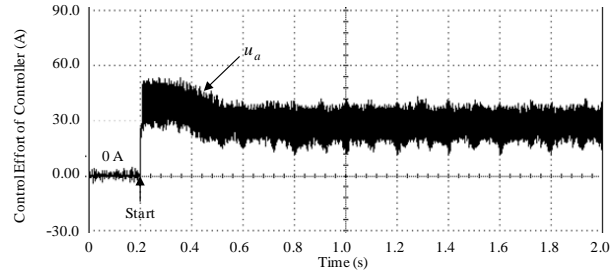


Fig. 11. Experimental result of the PI controller for a PMSM servo-drive electric scooter at 251.2 rad/s case with control effort response

desired rotor speed command  $\omega^*$  and the measured rotor speed  $\omega_c$  for a PMSM servo-drive electric scooter using the PID controller at 125.6 rad/s case is shown in Fig. 13. The zoom error of speed response for a PMSM servo-drive electric scooter using the PID controller at 125.6 rad/s is shown in Fig. 14. The current tracking response of the command current  $i_{ar}^*$  and measured current  $i_{ar}$  in phase  $a$  for a PMSM servo-drive electric scooter using the PID

controller at 125.6 rad/s case is shown in Fig. 15. The control effort  $u_a$  response for a PMSM servo-drive electric scooter using the PID controller at 125.6 rad/s case is shown in Fig. 16. The speed tracking response of the rotor speed command  $\omega_c^*$ , the desired rotor speed command  $\omega^*$  and the measured rotor speed  $\omega_c$  for a PMSM servo-drive electric scooter using the PID controller at 251.2 rad/s case is shown in Fig. 17. The zoom error of speed response for

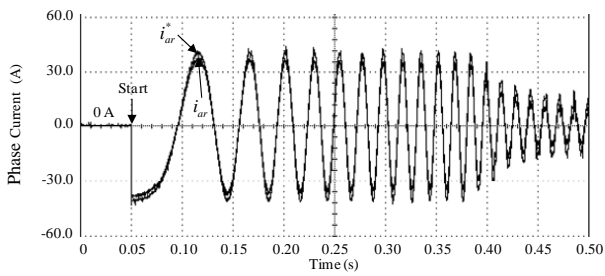


Fig. 12. Experimental result of the PI controller for a PMSM servo-drive electric scooter at 251.2 rad/s case with current tracking response

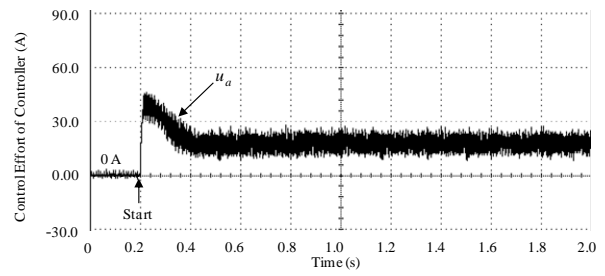


Fig. 15. Experimental result of the PID controller for a PMSM servo-drive electric scooter at 125.6 rad/s case with control effort response

a PMSM servo-drive electric scooter using the PID controller at 251.2 rad/s is shown in Fig. 18. The current tracking response of the command current  $i_{ar}^*$  and measured current  $i_{ar}$  in phase  $a$  for a PMSM servo-drive electric scooter using the PID controller at 251.2 rad/s case is shown in Fig. 19. The control effort  $u_a$  response for a PMSM servo-drive electric scooter using the PID controller at 251.2 rad/s case is shown in Fig. 20.

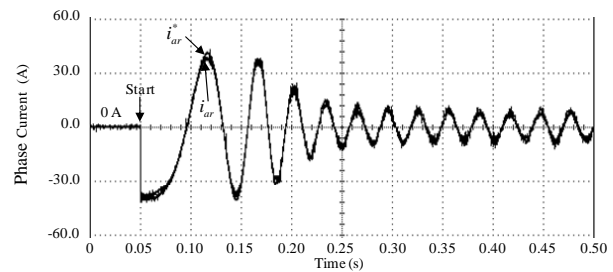


Fig. 16. Experimental result of the PID controller for a PMSM servo-drive electric scooter at 125.6 rad/s case with current tracking response

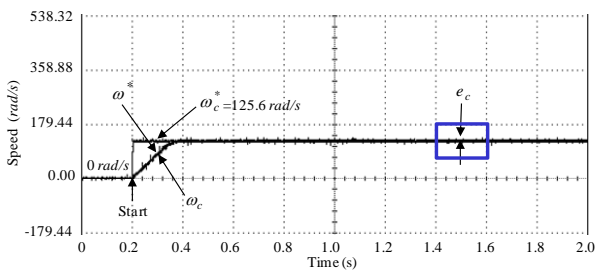


Fig. 13. Experimental result of the PID controller for a PMSM servo-drive electric scooter at 125.6 rad/s case with speed tracking response

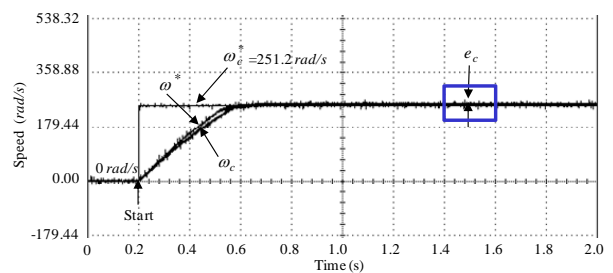


Fig. 17. Experimental result of the PID controller for a PMSM servo-drive electric scooter at 251.2 rad/s case for speed tracking response

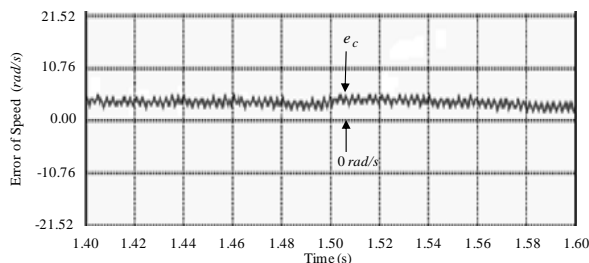


Fig. 14. Experimental result of the PID controller for a PMSM servo-drive electric scooter at 125.6 rad/s case with zoom error of speed response

Since the low speed operation is the same as the nominal case due to smaller the lumped external disturbances with parameter variations, the speed tracking responses using the PI and PID controllers shown in Figs. 5 and 13 have better tracking performance. But the zoom errors of speed using the PI and PID controllers shown in Figs. 6 and 14 are larger and slower convergence. The degenerate speed tracking responses using the PI controller and PID

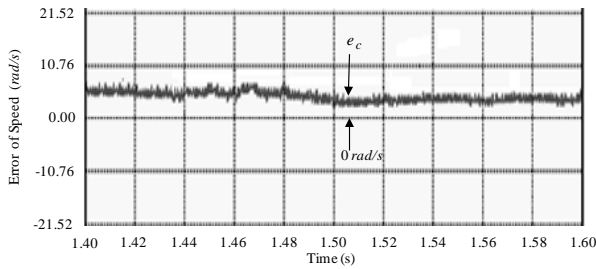


Fig. 18. Experimental result of the PID controller for a PMSM servo-drive electric scooter at 251.2 rad/s case with zoom error of speed response

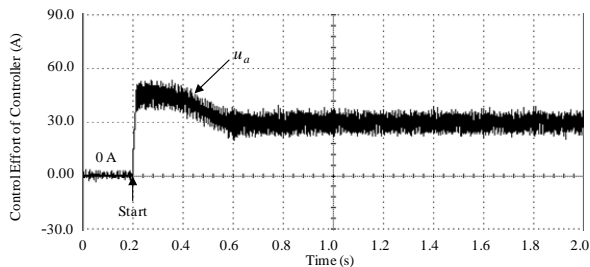


Fig. 19. Experimental result of the PID controller for a PMSM servo-drive electric scooter at 251.2 rad/s case with control effort response

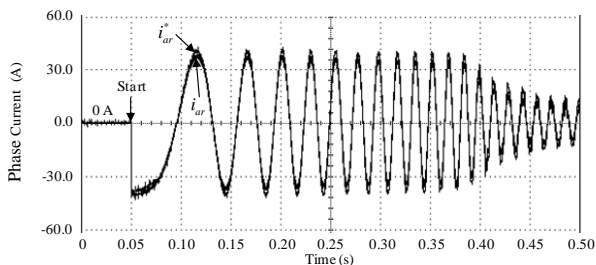


Fig. 20. Experimental result of the PID controller for a PMSM servo-drive electric scooter at 251.2 rad/s case with current tracking response

controllers shown in Figs. 9 and 17 resulted owing to the occurrence of the larger lumped external disturbances with parameter variations. In addition, the control efforts using the PI and PID controllers shown in Figs. 7, 11, 15 and 19 resulted larger chattering due to action on CVT system with nonlinear disturbance, such as belt shaking friction, nonlinear friction between primary pulley and second pulley. From the experimental results, sluggish speed tracking responses of the PI and PID controllers for a PMSM

servo-drive electric scooter are obtained owing to the weak robustness of the linear controller without online adjustment mechanism. Moreover, the PID controller provided faster response than the PI controller but often has harder to control and more sensitive to changes in the plant. The problems with noise in the PI controller are exacerbated by the use of a differential gain  $k_{ds}$  shown in Figs. 14, 15 and 16. To reduce the noise, lowering the frequency of the derivative's low-pass filter will help, but it will also limit the effectiveness of the differential gain  $k_{ds}$ . Noise can also be reduced by reducing the differential gain  $k_{ds}$  directly, but this is usually a poorer alternative than lowering the low-pass filter frequency.

For comparison with the proposed novel adaptive modified recurrent Legendre NN control system, the adopted three-layer feedforward NN control system with sigmoid activation function in the hidden layer has two, three and one neurons in the input layer, the hidden layer and the output layer, respectively. The experimental results of the three-layer feedforward NN control system controlled for a PMSM servo-drive electric scooter at 125.6 rad/s case and 251.2 rad/s case are shown in Figs. 21-28. The speed tracking response of the rotor speed command  $\omega_c^*$ , the desired rotor speed command  $\omega^*$  and the measured rotor speed  $\omega_c$  for a PMSM servo-drive electric scooter using the three-layer feedforward NN control system at 125.6 rad/s case is shown in Fig. 21. The zoom error of speed response for a PMSM servo-drive electric scooter using the three-layer feedforward NN control system at 125.6 rad/s is shown in Fig. 22. The current tracking response of the command current  $i_{ar}^*$  and measured current  $i_{ar}$  in phase *a* for a PMSM servo-drive electric scooter using the three-layer feedforward NN control system at 125.6 rad/s case is shown in Fig. 23. The control effort  $u_a$  response for a PMSM servo-drive electric scooter using the three-layer feedforward NN control system at 125.6 rad/s case is shown in Fig. 24.

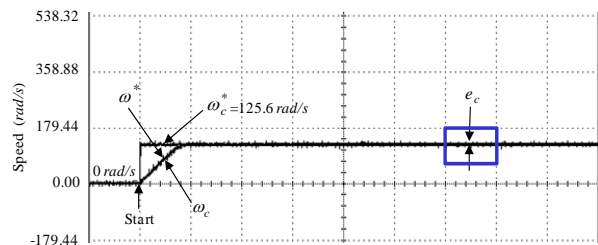


Fig. 21. Experimental result of the three-layer feedforward NN control system for a PMSM servo-drive electric scooter at 125.6 rad/s case with speed tracking response

The speed tracking response of the rotor speed com-

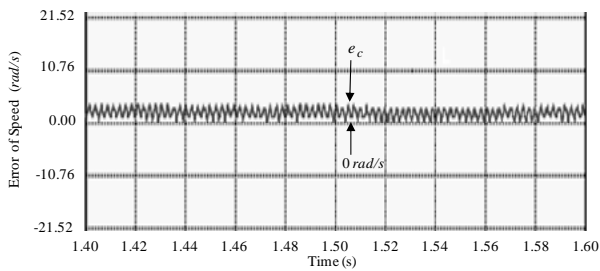


Fig. 22. Experimental result of the three-layer feedforward NN control system for a PMSM servo-drive electric scooter at 125.6 rad/s case with zoom error of speed response

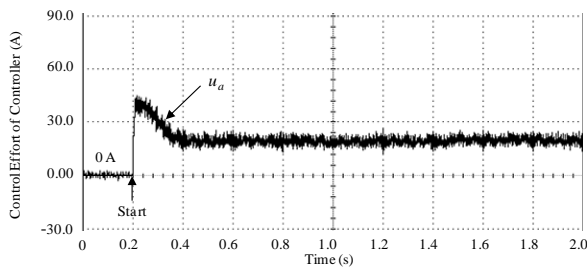


Fig. 23. Experimental result of the three-layer feedforward NN control system for a PMSM servo-drive electric scooter at 125.6 rad/s case with control effort response

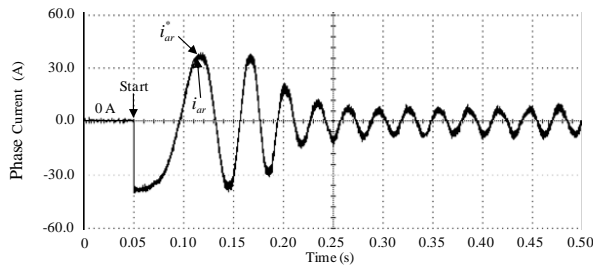


Fig. 24. Experimental result of the three-layer feedforward NN control system for a PMSM servo-drive electric scooter at 125.6 rad/s case with current tracking response

mand  $\omega_c^*$ , the desired rotor speed command  $\omega^*$  and the measured rotor speed  $\omega_c$  for a PMSM servo-drive electric scooter using the three-layer feedforward NN control system at 251.2 rad/s case is shown in Fig. 25. The zoom error of speed response for a PMSM servo-drive electric scooter using the three-layer feedforward NN control system at 251.2 rad/s is shown in Fig. 26. The current tracking response of the command current  $i_{ar}^*$  and measured current

$i_{ar}$  in phase  $a$  for a PMSM servo-drive electric scooter using the three-layer feedforward NN control system at 251.2 rad/s case is shown in Fig. 27. The control effort  $u_a$  response for a PMSM servo-drive electric scooter using the three-layer feedforward NN control system at 251.2 rad/s case is shown in Fig. 28.

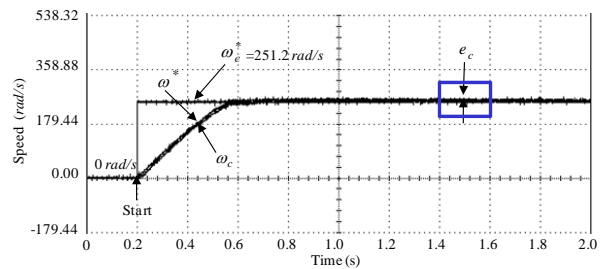


Fig. 25. Experimental result of the three-layer feedforward NN control system for a PMSM servo-drive electric scooter at 251.2 rad/s case with speed tracking response

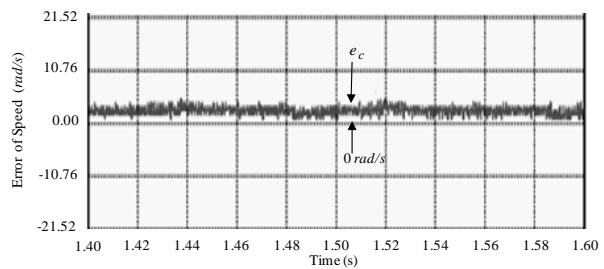


Fig. 26. Experimental result of the three-layer feedforward NN control system for a PMSM servo-drive electric scooter at 251.2 rad/s case with zoom error of speed response

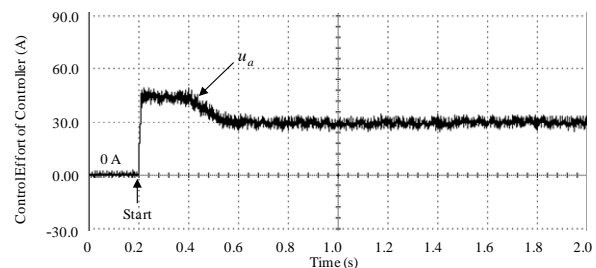


Fig. 27. Experimental result of the three-layer feedforward NN control system for a PMSM servo-drive electric scooter at 251.2 rad/s case with control effort response

The control gains of the proposed novel adaptive mod-

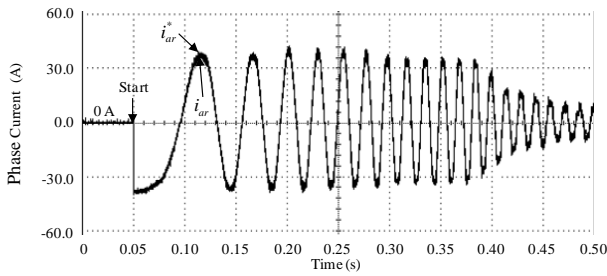


Fig. 28. Experimental result of the three-layer feedforward NN control system for a PMSM servo-drive electric scooter at 251.2 rad/s case with current tracking response

ified recurrent Legendre NN control system are selected as  $\eta = 0.2$  in order to achieve the best transient control performance in experimentation considering the requirement of stability. The parameter adjustment process remains continually active for the duration of the experimentation. The experimental results of the novel adaptive modified recurrent Legendre NN control system for a PMSM servo-drive electric scooter at 125.6rad/s case and 251.2rad/s case are shown in Figs. 29-36. The speed tracking response of the rotor speed command  $\omega_c^*$ , the desired rotor speed command  $\omega^*$  and the measured rotor speed  $\omega_c$  for a PMSM servo-drive electric scooter using the novel adaptive modified recurrent Legendre NN control system at 125.6 rad/s case is shown in Fig. 29. The zoom error of speed response for a PMSM servo-drive electric scooter using the novel adaptive modified recurrent Legendre NN control system at 125.6 rad/s is shown in Fig. 30. The current tracking response of the command current  $i_{ar}^*$  and measured current  $i_{ar}$  in phase  $a$  for a PMSM servo-drive electric scooter using the novel adaptive modified recurrent Legendre NN control system at 125.6 rad/s case is shown in Fig. 31. The control effort  $u_a$  response for a PMSM servo-drive electric scooter using the novel adaptive modified recurrent Legendre NN control system at 125.6 rad/s case is shown in Fig. 32. The speed tracking response of the rotor speed command  $\omega_c^*$ , the desired rotor speed command  $\omega^*$  and the measured rotor speed  $\omega_c$  for a PMSM servo-drive electric scooter using the novel adaptive modified recurrent Legendre NN control system at 251.2 rad/s case is shown in Fig. 33. The zoom error of speed response for a PMSM servo-drive electric scooter using the novel adaptive modified recurrent Legendre NN control system at 251.2 rad/s is shown in Fig. 34. The current tracking response of the command current  $i_{ar}^*$  and measured current  $i_{ar}$  in phase  $a$  for a PMSM servo-drive electric scooter using the novel adaptive modified recurrent Legendre NN control system at 251.2 rad/s case is shown in Fig. 35. The

control effort  $u_a$  response for a PMSM servo-drive electric scooter using the novel adaptive modified recurrent Legendre NN control system at 251.2 rad/s case is shown in Fig. 36.

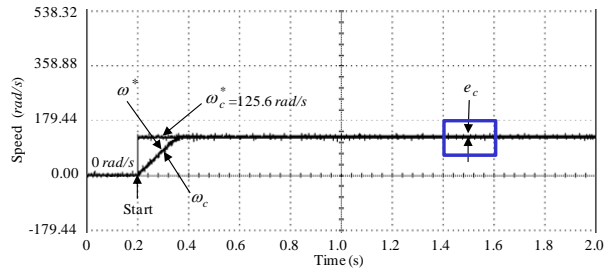


Fig. 29. Experimental result of the novel adaptive modified recurrent Legendre NN control system for a PMSM servo-drive electric scooter at 125.6 rad/s case with speed tracking response

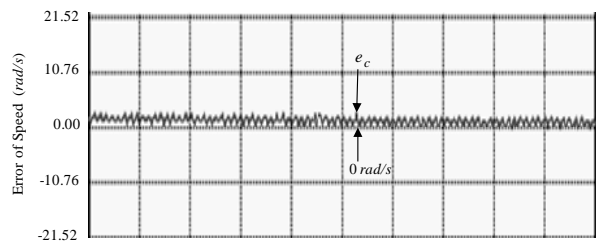


Fig. 30. Experimental result of the novel adaptive modified recurrent Legendre NN control system for a PMSM servo-drive electric scooter at 125.6 rad/s case with zoom error of speed response

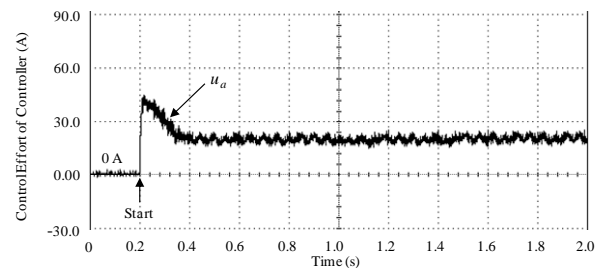


Fig. 31. Experimental result of the novel adaptive modified recurrent Legendre NN control system for a PMSM servo-drive electric scooter at 125.6 rad/s case with control effort response

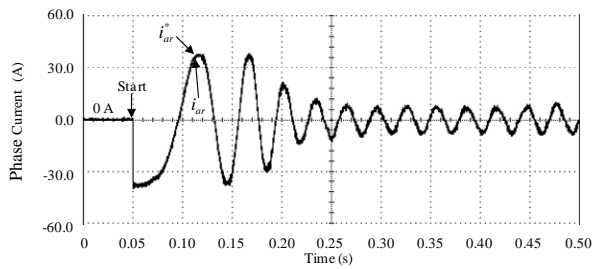


Fig. 32. Experimental result of the novel adaptive modified recurrent Legendre NN control system for a PMSM servo-drive electric scooter at 125.6 rad/s case with current tracking response

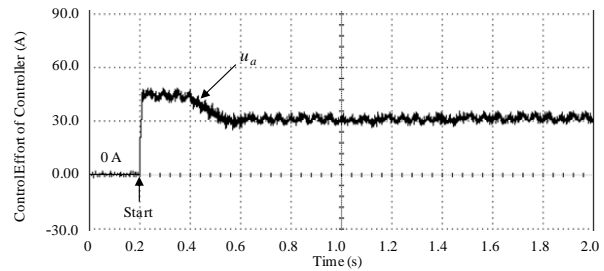


Fig. 35. Experimental result of the novel adaptive modified recurrent Legendre NN control system for a PMSM servo-drive electric scooter at 251.2 rad/s case with control effort response

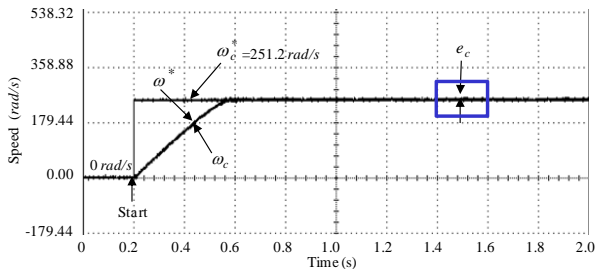


Fig. 33. Experimental result of the novel adaptive modified recurrent Legendre NN control system for a PMSM servo-drive electric scooter at 251.2 rad/s case with speed tracking response

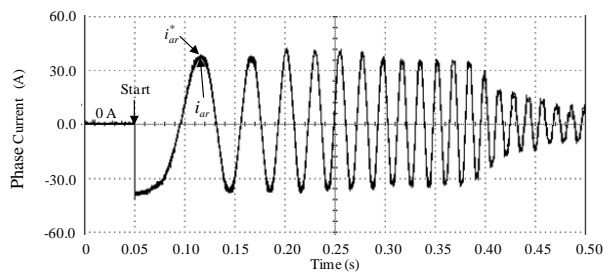


Fig. 36. Experimental results of the novel adaptive modified recurrent Legendre NN control system for a PMSM servo-drive electric scooter at 251.2 rad/s case with current tracking response

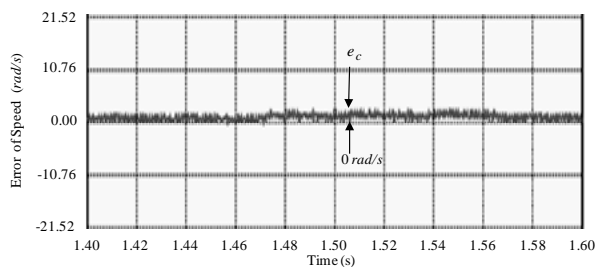


Fig. 34. Experimental result of the novel adaptive modified recurrent Legendre NN control system for a PMSM servo-drive electric scooter at 251.2 rad/s case with zoom error of speed response

Since the low speed operation is the same as the nominal case due to smaller the lumped external disturbances with parameters variations, the speed tracking responses for four control systems shown in Figs. 5, 13, 21 and 29 have better tracking performance. But the zoom errors of tracking speed using the PI controller and the PID

controller shown in Figs. 6 and 14 are larger than the three-layer feedforward NN control system and the novel adaptive modified recurrent Legendre NN control system shown in Figs. 22 and 30, respectively, due to online adjustment abilities of the three-layer feedforward NN control system and the modified recurrent Legendre NN control system. Meanwhile, the control efforts using the PI controller and the PID controller shown in Figs. 7, 11 and 15, 19 have larger chattering phenomena than the three-layer feedforward NN control system shown and the novel adaptive modified recurrent Legendre NN control system shown in Figs. 23, 27 and 31, 35, respectively. That is due to online adjustment abilities of the three-layer recurrent NN and the modified recurrent Legendre NN to cope with high frequency unmodeled dynamics of the controlled plant. In addition, the zoom errors of speed of the PI controller, the PID controller, the three-layer feedforward NN control system and the novel adaptive modified recurrent Legendre NN control system at 251.2 rad/s are shown in Figs. 10, 18, 26 and 34, respectively. From above experimental results, the novel adaptive modified recurrent

Legendre NN control system has smaller convergence error and faster dynamic response. However, owing to the online adaptive mechanism of modified recurrent Legendre NN and the remunerated controller, accurate tracking control performance of the PMSM can be obtained. These results show that the novel adaptive modified recurrent Legendre NN control system has better performance than the PI and PID controllers to speed perturbation for a PMSM servo-drive electric scooter. Additionally, the small chattering phenomena of the currents in phase *a* shown in Fig. 19, Fig. 22 and Fig. 25, Fig. 28 are induced by online adjustment of the three-layer feedforward NN and the modified recurrent Legendre NN to cope with highly nonlinear dynamics of system. Furthermore, the modified recurrent Legendre NN control system shown Figs. 30, 34 has faster convergence than the three-layer feedforward NN control system as comparison Fig. 30, Fig. 34 with Fig. 22, Fig. 26 due to lower computational complexity. Furthermore, the control efforts for the novel adaptive modified recurrent Legendre NN control system shown in Figs. 31, 35 have lower ripple than the three-layer feedforward NN control system shown in Figs. 23, 27 due to online adjustment mechanism of the modified recurrent Legendre NN to cope with high frequency unmodeled dynamics of the controlled plant and fast convergence capacity by using two vary learning rates.

In addition, the novel adaptive modified recurrent Legendre NN control system has faster dynamic response and faster convergence from the responses of the optimal learning rate of connective weight and the optimal learning rate of recurrent weight in the modified recurrent Legendre NN control at 125.6 *rad/s* case and 251.2 *rad/s* case shown in Figs. 37-38 and Figs. 39-40, respectively.

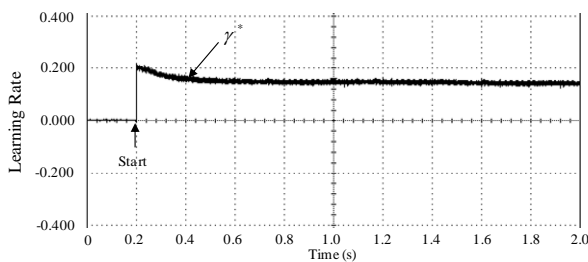


Fig. 37. Experimental result of the novel adaptive modified recurrent Legendre NN control system for a PMSM servo-drive electric scooter at 125.6 *rad/s* case with optimal learning rate of connective weight response

Finally, the measurement of load regulation under step disturbance torque is tested. The PI control, the PID control, the three-layer feedforward NN control system and the novel adaptive modified recurrent Legendre NN con-

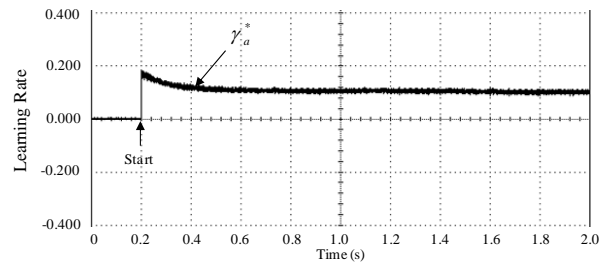


Fig. 38. Experimental result of the novel adaptive modified recurrent Legendre NN control system for a PMSM servo-drive electric scooter at 125.6 *rad/s* case with optimal learning rate of recurrent weight response

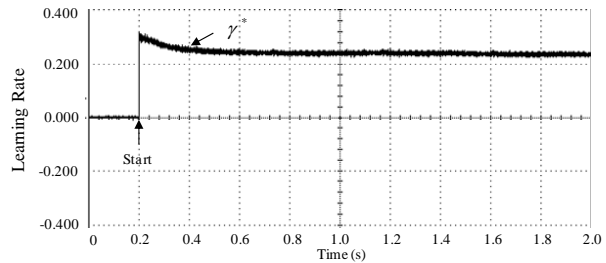


Fig. 39. Experimental result of the novel adaptive modified recurrent Legendre NN control system for a PMSM servo-drive electric scooter at 251.2 *rad/s* case with optimal learning rate of connective weight response

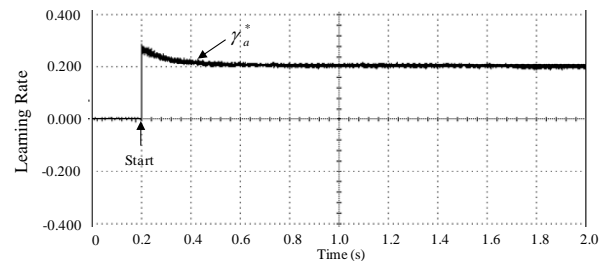


Fig. 40. Experimental result of the novel adaptive modified recurrent Legendre NN control system for a PMSM servo-drive electric scooter at 251.2 *rad/s* case with optimal learning rate of recurrent weight response

rol system are tested under  $T_l = 2 \text{ Nm}$  load torque disturbance with adding load and shedding load. The experimental results of the measured rotor speed responses and measured current in phase *a* using the PI controller, the PID controller, the three-layer feedforward NN control system and the novel adaptive modified recurrent Legendre

NN control system under  $T_l = 2 Nm$  load torque disturbance with adding load and shedding load at  $251.2 rad/s$  are shown in Figs. 41, 43, 45 and 47, respectively. The zoom errors of speed of the PI controller, the PID controller, the three-layer feedforward NN control system and the novel adaptive modified recurrent Legendre NN control system under  $T_l = 2 Nm$  load torque disturbance with adding load and shedding load at  $251.2 rad/s$  are shown in Figs. 42, 44, 46 and 48, respectively.

From the experimental result, the rotor degenerated response under the variation of rotor inertia and load torque disturbance is much improved by means of the novel adaptive modified recurrent Legendre NN control system. From experimental results, transient response of the novel adaptive modified recurrent Legendre NN control system is much better than the PI controller, the PID controller and the three-layer feedforward NN control system at load regulation. Moreover, the novel adaptive modified recurrent Legendre NN control system has faster convergence and better load regulation than the three-layer feedforward NN control system under the variation of rotor inertia and load torque.

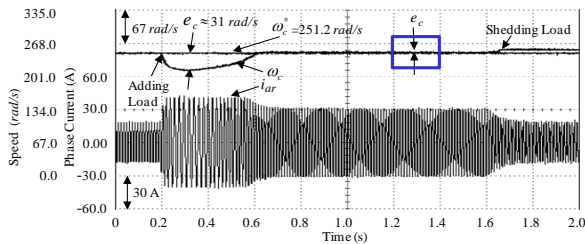


Fig. 41. Experimental result of the PI controller under  $T_l = 2 Nm$  load torque disturbance with adding load and shedding load at  $251.2 rad/s$  case for speed response and current response

### 5 CONCLUSION

A PMSM servo-drive electric scooter system controlled by the novel adaptive modified recurrent Legendre NN control system with online parameter adjustment and fast convergence has been successfully developed in this study.

Firstly, the dynamic models of the PMSM servo-drive electric scooter system were derived. Because the electric scooter is a nonlinear and time-varying system, sluggish speed tracking are obtained for the PI and PID controlled PMSM servo-drive electric scooter owing to the weak robustness of the linear controller. Therefore, the PMSM servo-drive electric scooter controlled by the novel adap-

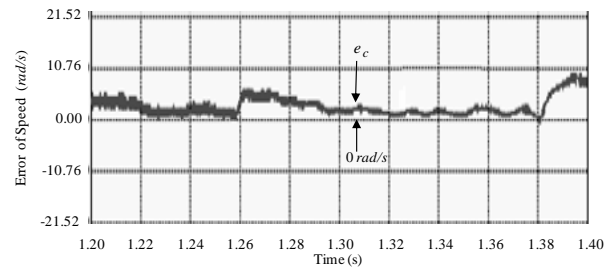


Fig. 42. Experimental result of the PI controller under  $T_l = 2 Nm$  load torque disturbance with adding load and shedding load at  $251.2 rad/s$  case for zoom error of speed response

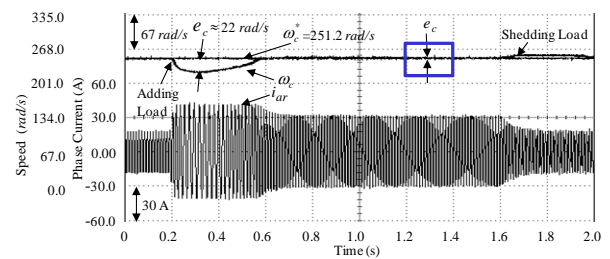


Fig. 43. Experimental result of the PID controller under  $T_l = 2 Nm$  load torque disturbance with adding load and shedding load at  $251.2 rad/s$  case for speed response and current response

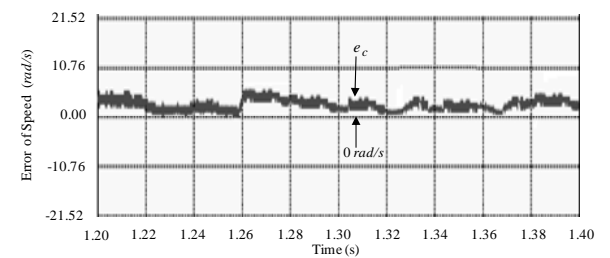


Fig. 44. Experimental result of the PID controller under  $T_l = 2 Nm$  load torque disturbance with adding load and shedding load at  $251.2 rad/s$  case for zoom error of speed response

tive modified recurrent Legendre NN control system is developed in order to raise robustness under the occurrence of the variation of rotor inertia and load torque disturbance.

Secondly, the online parameter tuning methodology of the modified recurrent Legendre NN and the estimation law of the remunerated controller are derived by using the

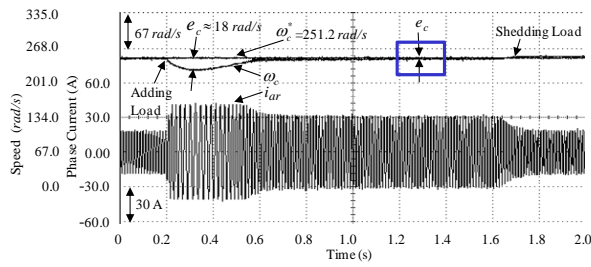


Fig. 45. Experimental result of the three-layer feedforward NN control system under  $T_l = 2 \text{ Nm}$  load torque disturbance with adding load and shedding load at 251.2 rad/s case for speed response and current response

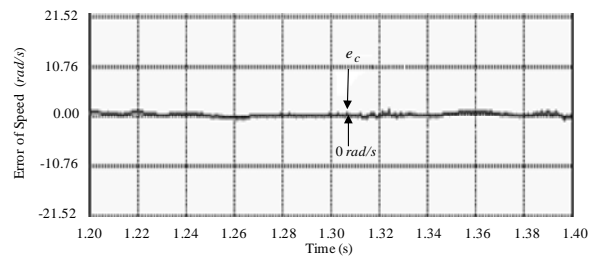


Fig. 48. Experimental result of the novel adaptive modified recurrent Legendre NN control system under  $T_l = 2 \text{ Nm}$  load torque disturbance with adding load and shedding load at 251.2 rad/s case for zoom error of speed response

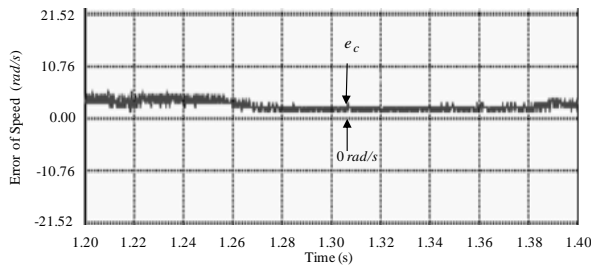


Fig. 46. Experimental result of the three-layer feedforward NN control system under  $T_l = 2 \text{ Nm}$  load torque disturbance with adding load and shedding load at 251.2 rad/s case for zoom error of speed response

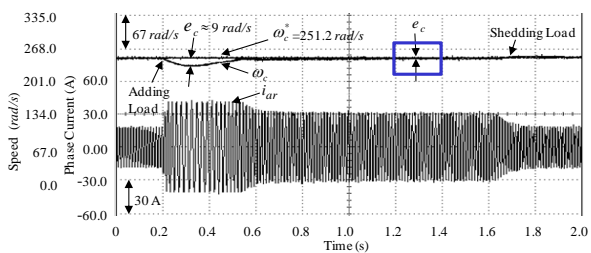


Fig. 47. Experimental result of the novel adaptive modified recurrent Legendre NN control system under  $T_l = 2 \text{ Nm}$  load torque disturbance with adding load and shedding load at 251.2 rad/s case for speed response and current response

Lyapunov stability theorem and gradient descent method.

In addition, the novel adaptive modified recurrent Legendre NN control system has faster convergence ability and better online learning capability than the three-layer feedforward NN control system in order to be able to fast cap-

ture the system's nonlinear and time-varying behaviors.

Moreover, the remunerated control with estimation law posed to remunerate the difference between ideal control and the modified recurrent Legendre NN control.

Finally, the control performance of the proposed novel adaptive modified recurrent Legendre control system is more suitable than the PI controller, the PID controller and the three-layer feedforward NN control system for the PMSM servo-drive electric scooter system from experimental results.

REFERENCES

- [1] D. W. Novotny, T. A. Lipo, *Vector control and dynamics of AC drives*, Oxford University Press, New York, 1996.
- [2] W. Leonhard, *Control of electrical drives*, Springer Verlag, Berlin, 1996.
- [3] F. J. Lin, "Real-time IP position controller design with torque feedforward control for PM synchronous motor," *IEEE Transactions on Industrial Electronics*, vol. 44, no. 3, pp. 398-407, June 1997.
- [4] S. Haykin, *Neural networks*, Maxwell Macmillan, Ottawa, ON, Canada, 1994.
- [5] P. S. Sastry, G. Santharam, K. P. Unnikrishnan, "Memory neural networks for identification and control of dynamical systems," *IEEE Transactions on Neural Networks*, vol. 5, no.2, pp. 306-319, March 1994.
- [6] R. Grino, G. Cembrano, C. Torras, "Nonlinear system identification using additive dynamic neural networks—two on-line approaches," *IEEE Transactions on Circuits Systems I*, vol. 47, no. 2, pp. 150-165, 2000.

- [7] A. Sarolic, P. Matic, "Wireless LAN electromagnetic field prediction for indoor environment using artificial neural network," *Automatika*, vol. 51, no. 3, pp. 233-140, 2010.
- [8] J. F. Carneiro and F. G. de Almeida, "A neural network based nonlinear model of a servopneumatic system," *ASME Journal of Dynamic Systems, Measurement, and Control*, vol. 134, no. 2, p.024502, March 2012.
- [9] Y. H. Pao, *Adaptive pattern recognition and neural networks*, Addison-Wesley, Boston, **Massachusetts, 1989**.
- [10] Y. H. Pao, S. M. Philips, "The functional link net and learning optimal control," *Neurocomputing*, vol. 9, no. 2, pp. 149-164, October 1995.
- [11] J. C. Patra, R. N. Pal, B. N. Chatterji, G. Panda, "Identification of nonlinear dynamic systems using functional link artificial neural networks," *IEEE Transactions on Systems, Man, and Cybernetics B*, vol. 29, no. 2, pp. 254-262, April 1999.
- [12] S. Dehuri, S. B. Cho, "A comprehensive survey on functional link neural networks and an adaptive PSOBP learning for CFLNN," *Neural Computing Applications*, vol. 19, no. 2, pp 187-205, March 2010.
- [13] S. S. Yang, C. S. Tseng, "An orthogonal neural network for function approximation," *IEEE Transactions on Systems, Man, and Cybernetics B*, vol. 26, no. 5, pp. 779-785, October 1996.
- [14] J. C. Patra, W. C. Chin, P. K. Meher, G. Chakraborty, "Legendre-FLANN-based nonlinear channel equalization in wireless communication systems," *Proceedings of the IEEE International Conferences on Systems, Man, Cybernetics*, Singapore, pp. 1826-1831, 2008.
- [15] J. C. Patra, P. K. Meher, G. Chakraborty, "Nonlinear channel equalization for wireless communication systems using Legendre neural networks," *Signal Processing*, vol. 89, no. 12, pp. 2251-2262, December 2009.
- [16] J. C. Patra, C. Bornand, "Nonlinear dynamic system identification using Legendre neural network," *Proceedings of the International Joint Conferences on Neural Networks*, Barcelona, Spain, pp. 1-7, 2010.
- [17] F. Liu, J. Wang, "Fluctuation prediction of stock market index by Legendre neural network with random time strength function," *Neurocomputing*, vol. 83, pp. 12-21, April 2012.
- [18] K. K. Das, J. K. Satapathy, "Novel algorithms based on Legendre neural network for nonlinear active noise control with nonlinear secondary path," *International Journal of Computer Science and Information Technologies*, vol. 3, no. 5, pp. 5036-5039, 2012.
- [19] R. K. Madyastha, B. Aazhang, "An algorithm for training multilayer perceptrons for data classification and function interpolation," *IEEE Transactions on Circuits Systems I*, vol. 41, no. 12, pp. 866-875, December 1994.
- [20] T. W. S. Chow, Y. Fang, "A recurrent neural-network-based real-time learning control strategy applying to nonlinear systems with unknown dynamics," *IEEE Transactions on Industrial Electronics*, vol. 45, no. 1, pp. 151-161, February 1998.
- [21] M. A. Brdys, G. J. Kulawski, "Dynamic neural controllers for induction motor," *IEEE Transactions on Neural Networks*, vol. 10, no. 2, pp. 340-355, March 1999.
- [22] X. D. Li, J. K. L. Ho, T. W. S. Chow, "Approximation of dynamical time-variant systems by continuous-time recurrent neural networks," *IEEE Transactions on Circuits Systems II*, vol. 52, no. 10, pp. 656-660, October 2005.
- [23] C. H. Lu, C. C. Tsai, "Adaptive predictive control with recurrent neural network for industrial processes: an application to temperature control of a variable-frequency oil-cooling machine," *IEEE Transactions on Industrial Electronics*, vol. 55, no. 3, pp. 1366-1375, March 2008.
- [24] Z. Maio, Y. Wang, "Robust dynamic surface control of flexible joint robots using recurrent neural networks," *Journal of Control Theory and Applications*, vol. 11, no. 2, pp. 222-229, May 2013.
- [25] R. Ortega, M. W. Spong, "Adaptive motion control of rigid robots: a tutorial," *Automatika*, vol. 25, no. 6, pp. 877-888, November 1998.
- [26] M. C. Chien, A. C. Huang, "Adaptive control for flexible-joint electrically driven robot with time-varying uncertainties," *IEEE Transactions on Industrial Electronics*, vol. 54, no. 2, pp.1032-1038, April 2007.
- [27] Z. G. Hou, A. M. Zou, L. Cheng, M. Tan, "Adaptive control of an electrically driven nonholonomic mobile robot via backstepping and fuzzy approach," *IEEE Transactions on Control Systems Technology*, vol. 17, no. 4, pp. 803-815, July 2009.

- [28] C. de. Sousa, Jr., E. M. Hemerly, R. K. H. Galvao, "Adaptive control for mobile robot using wavelet networks," *IEEE Transactions on Systems, Man, and Cybernetics B*, vol. 32, no. 4, pp. 493-504, August 2002.
- [29] S. N. Huang, K. K. Tan, T. H. Lee, "Adaptive neural network algorithm for control design of rigid-link electrically driven robots," *Neurocomputing*, vol. 71, no. 4-6, pp. 885-894, January 2008.
- [30] S. J. Yoo, J. B. Park, Y. H. Choi, "Adaptive output feedback control of flexible-joint robots using neural networks: dynamic surface design approach," *IEEE Transactions on Neural Networks*, vol. 19, no. 10, pp. 1712-1726, October 2008.
- [31] L. Cheng, Z. G. Hou, M. Tan, "Adaptive neural network tracking control for manipulators with uncertain kinematics, dynamics and actuator model," *Automatica*, vol. 45, no. 10, pp. 2312-2318, October 2009.
- [32] A. Farmanbordar, S. M. Hoseini, "Neural network adaptive output feedback control of flexible link manipulators," *ASME Journal of Dynamic Systems, Measurement, and Control*, vol. 135, no. 2, p. 021009, November 2013.
- [33] C. H. Lin, P. H. Chiang, C. S. Tseng, Y. L. Lin, M. Y. Lee, "Hybrid recurrent fuzzy neural network control for permanent magnet synchronous motor applied in electric scooter," *6th International Power Electronics Conference (IPEC 2010)*, Sapporo, Japan, pp. 1371-1376, 2010.
- [34] C. H. Lin, P. H. Chiang, C. S. Tseng, Y. L. Lin, M. Y. Lee, "Hybrid recurrent fuzzy neural network control for permanent magnet synchronous motor applied in electric scooter," *5th IEEE Conference on Industrial Electronics and Applications (ICIEA 2010)*, Taichung, Taiwan, pp. 2175-2180, 2010.
- [35] C. H. Lin, C. P. Lin, "The hybrid RFNN control for a PMSM drive system using rotor flux estimator," *International Journal of Power Electronics*, vol. 4, no. 1, pp. 33-48, 2012.
- [36] C. H. Lin, C. P. Lin, "The hybrid RFNN control for a PMSM electric scooter using rotor flux estimator," *Advances in Fuzzy Systems*, vol. 2012, art. no. 319828, 2012.
- [37] C. H. Lin, C. P. Lin, "The hybrid RFNN control for a PMSM drive electric scooter using rotor flux estimator," *International Journal of Electrical Power and Energy Systems*, vol. 51, pp. 213-223, October 2013.
- [38] C. H. Lin, C. P. Lin, "The hybrid RNN control for a PMSM drive system using rotor flux estimator," *Applied Mechanics and Materials*, vol. 145, pp. 542-546, February 2012.
- [39] C. H. Lin, "A novel hybrid recurrent wavelet neural network control for a PMSM drive electric scooter using rotor flux estimator," *International Review of Electrical Engineering*, vol. 7, no. 3, pp. 4486-4498, May 2012.
- [40] C. H. Lin, C. P. Lin, "A novel hybrid recurrent wavelet neural network control for a PMSM driven electric scooter," *Applied Mechanics and Materials*, vol. 284-287, pp. 2194-2198, February 2013.
- [41] C. H. Lin, "Hybrid recurrent wavelet neural network control of PMSM servo-drive system for electric scooter," *International Journal of Control Automation and Systems*, vol. 12, no. 1, pp. 177-187, February 2014.
- [42] C. H. Lin, C. P. Lin, "Hybrid modified Elman NN controller design on permanent magnet synchronous motor driven electric scooter," *Transactions of the Canadian Society for Mechanical Engineering*, vol. 37, no. 4, pp. 1127-1145, 2013.
- [43] C. Y. Tseng, L. W. Chen, Y. T. Lin, J. Y. Li, "A hybrid dynamic simulation model for urban scooters with a mechanical-type CVT," *IEEE International Conference on Automation and Logistics*, Qingdao, China, pp. 519-519, 2008.
- [44] C. Y. Tseng, Y. F. Lue, Y. T. Lin, J. C. Siao, C. H. Tsai, L. M. Fu, "Dynamic simulation model for hybrid electric scooters," *IEEE International Symposium on Industrial Electronics*, Seoul, Korea, pp. 1464-1469, 2009.
- [45] J. J. E. Slotine, W. Li, *Applied nonlinear control*, Prentice Hall, Englewood Cliffs, New Jersey, 1991.
- [46] K. J. Astrom, B. Wittenmark, *Adaptive control*, Addison Wesley, New York, 1995.
- [47] K. J. Astrom, T. Haggglund, *PID controller: theory, design, and tuning*, North Carolina: Instrument Society of America, Research Triangle Park, 1995.
- [48] T. Haggglund, K. J. Astrom, "Revisiting the Ziegler-Nichols tuning rules for PI control," *Asian Journal of Control*, vol. 4, no. 4, pp. 364-380, December 2002.
- [49] T. Haggglund, K. J. Astrom, "Revisiting the Ziegler-Nichols tuning rules for PI control— part II: the frequency response method," *Asian Journal of Control*, vol. 6, no. 4, pp. 469-482, December 2004.



**Chih-Hong Lin** was born in Taichung, Taiwan. He received his B.S. and M.S. in Electrical Engineering from National Taiwan University of Science and Technology, Taipei, Taiwan, R.O.C., in 1989 and 1991, respectively. He received his Ph.D. in Electrical Engineering from Chung Yuan Christian University, Chung Li, Taiwan, R.O.C., in 2001. He is currently an associate

Professor in the Department of Electrical Engineering at He is currently an associate Professor at the National United University in Miaoli, Taiwan, R.O.C. His research interests include power electronics, motor servo drives and intelligent control.

#### **AUTHORS' ADDRESSES**

**Chih-Hong Lin, Ph. D.**

**Department of Electrical Engineering,**

**National United University,**

**Miaoli 36003, Taiwan**

**email: [jhlin@nuu.edu.tw](mailto:jhlin@nuu.edu.tw) Addresses: No. 1, Lienda,**

**Kung-Jing Li, Miaoli 36003, Taiwan**

Received: 2014-01-27

Accepted: 2014-08-01